Evolution of the angular momentum of protogalaxies from tidal torques: Zel'dovich approximation

Paolo Catelan and Tom Theuns

Department of Physics, Astrophysics, University of Oxford, Keble Road, Oxford OX1 3RH, UK

1 February 2008

ABSTRACT

The growth of the angular momentum $\mathbf{L}$ of protogalaxies induced by tidal torques is reconsidered. We adopt White's formalism and study the evolution of $\mathbf{L}$ in Lagrangian coordinates; the motion of the fluid elements is described by the Zel'dovich approximation. We obtain a general expression for the ensemble expectation value of the square of $\mathbf{L}$ in terms of the first and second invariant of the inertia tensor of the Lagrangian volume Γ enclosing the protoobject's collapsing mass. We then specialize the formalism to the particular case in which Γ is centred on a peak of the smoothed Gaussian density field and approximated by an isodensity ellipsoid. The result is the appropriate analytical estimate for the rms angular momentum of peaks to be compared against simulations that make use of the Hoffman-Ribak algorithm to set up a constrained density field that contains a peak with given shape. Extending the work of Heavens & Peacock, we calculate the *joint* probability distribution function for several spin parameters and peak mass M using the distribution of peak shapes, for different initial power spectra. The probability distribution for the rms final angular momentum $\langle \mathbf{L}_f^2 \rangle^{1/2}$ on the scales corresponding to common bright galaxies, $M \approx 10^{11} M_\odot$, is centred on a value of $\approx 10^{67} \, \mathrm{kg \, m^2 \, s^{-1}}$, for any cosmologically relevant power spectrum, in line with previous theoretical and observational estimates for L_f. Other astrophysical consequences are discussed. In particular, we find that typical values $\langle \lambda^2 \rangle^{1/2} \approx 0.1$ of the dimensionless spin parameter for peaks smoothed on galactic scales and of height $\nu \sim 1$, usually associated with late type galaxies, may be recovered in the framework of the Gaussian peak formalism. This partially relaxes the importance attributed to dissipative processes in generating such high values of centrifugal support for spiral galaxies. In addition, the values of the specific angular momentum versus mass – as deduced from observations of rotational velocities and photometric radii of spiral galaxies – are well fitted by our theoretical isoprobability contours. In contrast, the observed lower values for the specific angular momentum for ellipticals of the same mass cannot be accounted for within our linear regime investigation, highlighting the importance of strongly non-linear phenomena to explain the spin of such objects.

Key words: galaxies: formation – large–scale structure of the Universe

1 INTRODUCTION

It has been argued that tidal coupling between the inhomogeneities in the primordial matter distribution, in the context of a gravitational hierarchical scenario, may explain the acquisition of the angular momentum by a protogalaxy. This idea, originally due to Hoyle (1949) and applied by Sciama (1955), has been first thoroughly examined by Peebles (1969), who demonstrated that the tidal spin growth of the matter contained in a spherical (Eulerian) volume is proportional to $t^{5/3}$ in an Einstein–de Sitter universe (t is the standard cosmic time). Specifically, Peebles' analysis is based on a *second-order* perturbative description, since a spherical volume does not gain angular momentum from tidal torques in linear approximation, as pointed out by Zel'dovich and reported by Doroshkevich (1970). An important result of Doroshkevich's paper is that a *generic nonspherical* volume enclosing the protogalaxy acquires tidal angular momentum proportionally to the cosmic time

t during the linear regime. This theoretical prediction has been confirmed by the N–body simulations of White (1984). In addition, White showed that the second-order growth described by Peebles is due to convective motion of matter across the surface of the initial volume Γ containing the protoobject. An important point of Peebles and White's theoretical analyses is that they describe the tidal torques acting on a volume centred on a *random* point in the smoothed density field, which does not necessarily enclose a bound protogalaxy. In contrast, galaxies are expected to form around (high) peaks on relevant scales in the density field. This idea, in embryo in Doroshkevich (1970), developed into the biased galaxy formation scenario, where only density maxima above a given threshold (peaks) of the initial Gaussian density field can eventually form galaxies (Kaiser 1984; Politzer & Wise 1984; Peacock & Heavens 1985; Bardeen et al. 1986).

The acquisition of angular momentum due to tidal torques by Gaussian high–density peaks has been recently analyzed, amongst others, by Hoffman (1986; 1988), Heavens & Peacock (1988), Ryden (1988), Quinn & Binney (1992) and Eisenstein & Loeb (1995). Comparisons with N–body simulations are displayed in Efstathiou & Jones (1979), Barnes & Efstathiou (1987) and Warren et al. (1992).

In this paper, we re-examine the growth during the linear regime of the angular momentum $\mathbf{L}$ of protogalaxies induced by tidal couplings with the surrounding matter inhomogeneities. The layout of this article is the following. In the next section we briefly review White's formalism describing the linear evolution of tidal galactic spin. The motion of the mass fluid elements is described by the Zel'dovich approximation: the invariance of the angular momentum with respect to the Eulerian and Lagrangian description is stressed. Next, we derive a general (but approximate) expression for the ensemble expectation value of the square of $\mathbf{L}$, $\langle \mathbf{L}^2 \rangle$, in terms of the first and second invariant of the inertia tensor of the Lagrangian volume Γ. We then specialize our formalism to the particular case in which the Lagrangian volume is centred on a peak of the underlying smoothed Gaussian density field and approximated by an isodensity profile ellipsoid: in this case, we obtain the correct constrained ensemble average for these objects with preselected inertia tensor. The result is the appropriate analytical estimate for the rms angular momentum of peaks to be compared against simulations that make use of the Hoffman-Ribak algorithm to set up a constrained density field that contains a peak with given shape (Hoffman & Ribak 1991; van de Weygaert & Bertschinger 1996). Extending the work of Heavens & Peacock, we calculate the *joint* probability distribution function for several spin parameters (angular momentum, specific angular momentum, angular momentum in units of $M^{5/3}$) and peak mass M using the distribution of peak shapes (Bardeen et al. 1986), for different density power spectra. Finally, we discuss astrophysical implications in the last section. Technical details are given in appendices.

2   ANGULAR MOMENTUM

We carry out our analysis of the evolution of the angular momentum in three steps: first, we review White's method for obtaining an expression for $\mathbf{L}$ involving the shape of the protoobject and the distribution of the surrounding matter. Next, we simplify the expression for $\mathbf{L}$ by performing the ensemble average in subsection 2.2. Finally, we specialize the formalism to the case where the object is centered on a peak of the (Gaussian) underlying density distribution.

2.1   Dynamical description

Let us assume that at the epoch of structure formation the matter may be described on the relevant scales as a Newtonian collisionless cold fluid (dust) embedded in an expanding Friedmann universe with arbitrary density parameter Ω (but, for simplicity, vanishing cosmological constant). We indicate the comoving Eulerian spatial coordinate by $\mathbf{x}$. The physical distance is $\mathbf{r} = a(t)\mathbf{x}$, with $a(t)$ the expansion scale factor. In the Einstein–de Sitter model, $a(t) \propto t^{2/3}$.

The angular momentum $\mathbf{L}$ of the matter contained at time t in a volume V of the Eulerian $\mathbf{x}$-space is

$$\mathbf{L}(t) = \int_{a^3 V} d\mathbf{r}\, \rho \mathbf{r} \times \mathbf{v} = \rho_b a^4 \int_V d\mathbf{x}\, (1 + \delta)\mathbf{x} \times \mathbf{u} \,. \tag{1}$$

Here, $\rho = \rho_b(1+\delta)$ denotes the matter density field, ρ_b the background mean density, δ the density fluctuation field; $\mathbf{v} = d\mathbf{r}/dt$ indicates the velocity field and $\mathbf{u} = a\, d\mathbf{x}/dt$ is the so called "peculiar" velocity (see, e.g., Peebles 1980). The origin of the Cartesian coordinate system is assumed to coincide with the centre of mass. Since we are interested in the intrinsic angular motion, we disregard the centre–of–mass motion.

It is important to note that the previous integral over the *Eulerian* volume V may equally be written as an integral over the corresponding *Lagrangian* volume Γ:

$$\mathbf{L}(t) = \eta_0\, a^2 \int_\Gamma d\mathbf{q}\, (\mathbf{q} + \mathbf{S}) \times \frac{d\mathbf{S}}{dt} \,, \tag{2}$$

where $\rho_b a^3 = \rho_0 a_0^3 \equiv \eta_0$ in the matter dominated era. Equation (2) can be obtained from equation (1) using the mapping

$$\mathbf{x}(\mathbf{q}, t) = \mathbf{q} + \mathbf{S}(\mathbf{q}, t) \,, \tag{3}$$

from Lagrangian coordinates $\mathbf{q}$ to Eulerian coordinates $\mathbf{x}$, where $\mathbf{S}$ is the displacement vector. The determinant J of the Jacobian of the mapping $\mathbf{q} \to \mathbf{x}(\mathbf{q}, t)$, $d\mathbf{x} \, J^{-1} = d\mathbf{q}$, is related to the density fluctuation through the continuity equation:

$$1 + \delta[\mathbf{x}(\mathbf{q}, t), t] = J(\mathbf{q}, t)^{-1} \,. \tag{4}$$

Before the occurrence of shell crossing (caustic formation process) J is non vanishing (see, e.g., Shandarin & Zel'dovich 1989).

The expression for $\mathbf{L}(t)$ in equation (2) allows us to apply the *Lagrangian* theory directly: we stress that it is an *exact* relation. Consequently, when applying perturbation theory to equation (3), perturbative corrections to $\mathbf{S}$ (Bouchet et al. 1992; Buchert 1994; Catelan 1995 and references therein) provide perturbative corrections to $\mathbf{L}$ (Catelan & Theuns 1996). Furthermore, equation (2) shows that $\mathbf{L}(t)$ depends on the shape of the Lagrangian volume Γ, which encloses, by definition, all the fluid elements that eventually form the galaxy. The boundary of a given condensation region Γ depends on the particular realisation of the density field and in general it may be extremely fuzzy.

The linear Lagrangian theory corresponds to the Zel'dovich approximation,

$$\mathbf{S}(\mathbf{q}, t) \approx \mathbf{S}^{(1)}(\mathbf{q}, t) = D(t) \nabla \psi_1(\mathbf{q}), \tag{5}$$

which coincides with the linear Eulerian approximation to first order in the spatial positions, and gives a qualitative correct quasi–nonlinear solution by extrapolating the straight trajectories of equation (5) beyond the range of strict validity (Zel'dovich 1970a, b; Shandarin & Zel'dovich 1989). The temporal function $D(t)$ describes the growing mode of the density perturbations: in the Einstein–de Sitter model $D(t) \propto a(t)$. We neglect the decaying mode.

The potential $\psi_1(\mathbf{q})$ is the linear gravitational potential (see the discussion in Kofman 1991): if $\tilde{\psi}_1(\mathbf{p}) \equiv \int d\mathbf{q} \, \psi_1(\mathbf{q}) \, \mathrm{e}^{-i\,\mathbf{p}\cdot\mathbf{q}}$ is the Fourier transform of the gravitational potential, then the Fourier transform $\tilde{\delta}_1(\mathbf{p})$ of the linear density field $\delta^{(1)}(\mathbf{q}, t) = D(t)\delta_1(\mathbf{q})$ is related to $\tilde{\psi}_1(\mathbf{p})$ via the Poisson equation, $\tilde{\delta}_1(\mathbf{p}) = p^2 \, \tilde{\psi}_1(\mathbf{p})$, where $p \equiv |\mathbf{p}|$, and $\mathbf{p}$ is the comoving Lagrangian wavevector.

In the Zel'dovich approximation, the exact equation (2) simplifies to:

$$\mathbf{L}(t) \approx \mathbf{L}^{(1)}(t) = \eta_0 \, a^2 \int_\Gamma d\mathbf{q} \left(\mathbf{q} + \mathbf{S}^{(1)} \right) \times \frac{d\mathbf{S}^{(1)}}{dt} = \eta_0 \, a^2 \frac{dD}{dt} \int_\Gamma d\mathbf{q} \, \mathbf{q} \times \nabla \psi_1(\mathbf{q}) \,. \tag{6}$$

As in White (1984), if it is assumed that $\psi_1(\mathbf{q})$ is adequately represented in the generic volume Γ by the first three terms of the Taylor series about the origin $\mathbf{q} = \mathbf{0}$, then each component $L_\alpha^{(1)}(t)$ may be written in a compact form as (White 1984)

$$L_\alpha^{(1)}(t) = a(t)^2 \dot{D}(t) \, \epsilon_{\alpha\beta\gamma} \, \mathcal{D}_{\beta\sigma}^{(1)} \, \mathcal{J}_{\sigma\gamma} \,, \tag{7}$$

once the deformation tensor at the origin $\mathbf{q} = \mathbf{0}$

$$\mathcal{D}_{\beta\sigma}^{(1)} \equiv \mathcal{D}_{\beta\sigma}^{(1)}(\mathbf{0}) = \partial_\beta \partial_\sigma \psi_1(\mathbf{0}) \,, \tag{8}$$

and the inertia tensor of the mass contained in the volume Γ

$$\mathcal{J}_{\sigma\gamma} \equiv \eta_0 \int_\Gamma d\mathbf{q} \, q_\sigma \, q_\gamma \,, \tag{9}$$

are introduced. The dot in equation (7) represents the operator d/dt, the symbol $\partial_\alpha \equiv \partial/\partial q_\alpha$ and $\epsilon_{\alpha\beta\gamma}$ is the completely antisymmetric Levi–Civita tensor, $\epsilon_{123} = 1$. Summation over repeated Greek indices is understood.

Equation (7) shows that the linear angular momentum $\mathbf{L}^{(1)}$ is in general non-zero because the principal axes of the inertia tensor $\mathcal{J}_{\alpha\beta}$, which depend only on the (irregular) shape of the volume Γ, are not aligned with the principal axes of the deformation tensor $\mathcal{D}_{\alpha\beta}^{(1)}$, which depend on the location of neighbour matter fluctuations (see the discussion in White 1984). This fact can be illustrated by writing explicitly one component of $\mathbf{L}$ in the inertia tensor's principal-axes system, e.g., $L_1^{(1)} \propto \mathcal{D}_{23}^{(1)} (\mathcal{J}_{33} - \mathcal{J}_{22})$: only the *off-diagonal* elements of the deformation tensor enter.

In addition, the time dependence of $\mathbf{L}^{(1)}$ is governed by the function $a(t)^2 \dot{D}(t)$, which simplifies to $\frac{2}{3} t_0^{-2} t$ in the Einstein–de Sitter universe, as first noted by Doroshkevich (1970) (the convention $a = D = (t/t_0)^{2/3}$ is adopted). Finally, we emphasize the spherical case: if Γ is a spherical Lagrangian volume, then $\mathcal{J}_{\sigma\gamma} = \frac{4\pi}{15} \eta_0 \, q^5 \, \delta_{\sigma\gamma}$ and $L_\alpha^{(1)} \propto \epsilon_{\alpha\beta\gamma} \mathcal{D}_{\beta\gamma}^{(1)} = 0$; the symbol $\delta_{\alpha\beta}$ indicates the Kronecker tensor. Consequently, the matter initially contained in a spherical volume does not gain any tidal spin during the linear regime (see the discussion in White 1984). Of course, as we will show in the next section, this also holds for the variance, i.e., $\langle \mathbf{L}_{sphere}^{(1)2} \rangle = 0$.

Note that the angular momentum $L_\alpha^{(1)}$ may be written directly in terms of the gravitational tidal field (which coincides with the shear field in the linear regime)

$$\mathcal{E}_{\beta\sigma}^{(1)} \equiv \mathcal{D}_{\beta\sigma}^{(1)} - \frac{1}{3} D^{-1} (\nabla \cdot \mathbf{S}^{(1)}) \delta_{\beta\sigma} = (\partial_\beta \partial_\sigma - \frac{1}{3} \delta_{\beta\sigma} \nabla^2) \psi_1 \,, \tag{10}$$

as

$$L_\alpha^{(1)}(t) = a(t)^2 \dot{D}(t) \, \epsilon_{\alpha\beta\gamma} \, \mathcal{E}_{\beta\sigma}^{(1)} \, \mathcal{J}_{\sigma\gamma} \,, \tag{11}$$

since the isotropic part of the deformation tensor does not contribute to the antisymmetric tensor product: this justifies the use of *tidal* angular momentum to indicate the angular momentum originated by the coupling between the *traceless* part of the deformation tensor and the inertia tensor.

Finally, one can express the initial deformation tensor $\mathcal{D}^{(1)}_{\alpha\beta}$ as an integral in Fourier space:

$$\mathcal{D}^{(1)}_{\alpha\beta} = -\int \frac{d\mathbf{p}}{(2\pi)^3}\, p_\alpha\, p_\beta\, \tilde{\psi}_1(\mathbf{p})\, \widetilde{W}(pR)\ . \tag{12}$$

Note that, here and hereafter, we are explicitly assuming that the potential field ψ_1 is filtered on scale R by means of the window function $W_R(\mathbf{q})$. The function $\widetilde{W}(pR)$ is the Fourier transform of the smoothing function $W_R(\mathbf{q})$. The filtering of the field ψ_1 on an appropriate scale reflects the restriction to the linear evolution of the protogalaxy, since the non-linear coupling between different modes is filtered out.

As far as one considers the evolution of a single collapsing region of assigned enclosing volume Γ and velocity field, then, to calculate its final angular momentum acquired via tidal couplings with the neighbour matter distribution, it is enough to supplement the equation (7) with the time t_M at which the perturbation stops expanding and starts to collapse. After t_M the angular momentum essentially stops growing, becoming less sensitive to tidal couplings (Peebles 1969). While for a general aspherical perturbation the epoch t_M is not well defined (see Eisenstein & Loeb 1995 for the case of an ellipsoid), if one restricts study to a spherical top–hat region with uniform overdensity $\bar{\delta} = \frac{3}{20}(6\pi t/t_M)^{2/3}$, then the time of maximum expansion is reached when $\bar{\delta} = \frac{3}{20}(6\pi)^{2/3}$ (see Peebles 1980).

However, one is interested in calculating the tidal galactic spin averaged over an *ensemble* of realizations of the gravitational potential random field ψ_1, rather than in the evolution of the single perturbation. This is particularly important in order to compare the results from N–body simulations against theoretical ones. This programme is carried out in the next section.

2.2 Ensemble average

We simplify the previous results by considering the expectation value of the square of $\mathbf{L}$, $\langle \mathbf{L}^2 \rangle_\psi$. In linear theory this is quite simple to do because $\langle \mathbf{L}^2 \rangle_\psi = \langle \mathbf{L}^{(1)2} \rangle_\psi$. Here and hereafter, we indicate the *linear* angular momentum simply by $\mathbf{L}$, and the initial gravitational potential by $\psi \equiv \psi_1$.

From the expression (7) of L_α, we obtain

$$\langle \mathbf{L}^2 \rangle_\psi = a^4 \dot{D}^2\, \epsilon_{\alpha\beta\gamma}\, \epsilon_{\alpha\beta'\gamma'}\, \langle \mathcal{J}_{\sigma\gamma}\, \mathcal{J}_{\sigma'\gamma'}\, \mathcal{D}_{\beta\sigma}\mathcal{D}_{\beta'\sigma'} \rangle_\psi \approx a^4 \dot{D}^2\, \epsilon_{\alpha\beta\gamma}\, \epsilon_{\alpha\beta'\gamma'}\, \mathcal{J}_{\sigma\gamma}\, \mathcal{J}_{\sigma'\gamma'}\, \langle \mathcal{D}_{\beta\sigma}\mathcal{D}_{\beta'\sigma'} \rangle_\psi\ . \tag{13}$$

Note that the correct procedure to compute $\langle \mathbf{L}^2 \rangle_\psi$ would require complete understanding of how the different realizations of ψ stochastically influence the boundary of the generic volume Γ, which in turn determines the inertia tensor $\mathcal{J}$. This is a major unsolved problem. To bypass it, we have assumed in the last step of equation (13) that $\mathcal{J}$ is uncorrelated with ψ, thereby simplifying the calculation considerably; the price to pay is a loss of accuracy. This approximation is equivalent to preselecting a volume with given inertia tensor and independently assigning the realizations of the field, or, from a different point of view, the last step of equation (13) would be strictly *correct* if the random field ψ were to be restricted to those realizations of the ensemble which are compatible with the preselected inertia tensor and one would restrict study to those objects only. For example, the Hoffman-Ribak algorithm (Hoffman & Ribak 1991; van de Weygaert & Bertschinger 1996; Sheth 1995) can be used to set up constrained realizations of the (Gaussian or non-Gaussian) random density field containing objects with a given inertia tensor.

In the context of the Gaussian peak formalism (section 2.3 and Appendix B), it is possible to compute exactly the (small) factor by which the neglect of correlation between inertia tensor and the gravitational potential in equation (13) leads to an overestimate of the rms angular momentum. Nevertheless, we prefer to maintain the present procedure in this section, both for its simplicity and because it is applied when calculating perturbative corrections to the linear tidal angular momentum, whose distribution deviates non-trivially from the Gaussian one during the mildly non-linear regime (Catelan & Theuns 1996; see also the last paragraph in Appendix B).

The ensemble average in equation (13) can be reduced to an integral over the initial power spectrum $P_\psi(k)$ using equation (12):

$$\langle \mathcal{D}_{\beta\sigma}\mathcal{D}_{\beta'\sigma'} \rangle_\psi = \int \frac{d\mathbf{p}}{(2\pi)^3}\, p_\beta\, p_\sigma\, p_{\beta'}\, p_{\sigma'}\, P_\psi(p)\, \widetilde{W}(pR)^2\ , \tag{14}$$

where $\langle \tilde{\psi}(\mathbf{p})\tilde{\psi}(\mathbf{p}') \rangle_\psi \equiv (2\pi)^3 \delta_D(\mathbf{p} + \mathbf{p}') P_\psi(p)$: the presence of the Dirac function is necessary to guarantee that the density power spectrum has the correct units of volume and the conservation of momentum in Fourier space.

Observing that in the integral (14) the function $P_\psi(p)\, \widetilde{W}(pR)^2$ depends only on the modulus p of the wavevector $\mathbf{p}$, and that the volume filtered by the window function $\widetilde{W}(pR)$ is spherically symmetric, applying the general relation

$$\int_{sphere} d\mathbf{p}\, p_\alpha\, p_\beta\, p_\gamma\, p_\delta\, F(|\mathbf{p}|) = \frac{4\pi}{15}(\delta_{\alpha\beta}\,\delta_{\gamma\delta} + \delta_{\alpha\gamma}\,\delta_{\beta\delta} + \delta_{\alpha\,\delta}\,\delta_{\beta\,\gamma}) \int dp\, p^6\, F(p)\,, \tag{15}$$

which holds for any function $F(p)$ depending only on the radius p, we finally obtain (see Appendix A for a detailed derivation) the particularly simple result

$$\langle \mathbf{L}^2 \rangle_\psi = \frac{2}{15} a^4 \dot{D}^2 (\mu_1^2 - 3\mu_2)\, \sigma_0(R)^2\,. \tag{16}$$

This result holds for any power spectrum $P_\psi(p)$ and is independent of the statistics of the underlying field. The quantity $\sigma_0(R)^2$ is the mass variance on the scale R, i.e. $\sigma_0(R)^2 \equiv (2\pi^2)^{-1} \int_0^\infty dp\, p^6\, P_\psi(p)\widetilde{W}(pR)^2$.

The general expression (16) is *independent* of the details of the shape of the boundary surface of the volume Γ: it depends only on the quantities μ_1 and μ_2, which are respectively the first and the second invariant of the inertia tensor $\mathcal{J}_{\alpha\beta}$. The latter are defined in terms of the eigenvalues ι_1, ι_2 and ι_3 of the inertia tensor,

$$\mu_1 \equiv \iota_1 + \iota_2 + \iota_3\,, \tag{17}$$

$$\mu_2 \equiv \iota_1\iota_2 + \iota_1\iota_3 + \iota_2\iota_3\,. \tag{18}$$

(The third invariant is the determinant, $\iota_1\iota_2\iota_3$.) We stress that the particular combination $\mu_1^2 - 3\mu_2$ is null for a sphere, since $\iota_1 = \iota_2 = \iota_3$ for a spherical volume Γ, whereas for a non-spherical volume, $\mu_1^2 - 3\mu_2 > 0$.

So far we have described the tidal torques acting on a volume centred on a *random* point in the smoothed density field, which does not necessarily enclose a bound protogalaxy. However, galaxies are expected to form around (high) peaks on relevant scales in the density field: in the biased galaxy formation scenario, only the density maxima above a given threshold (peaks) of the initial Gaussian density field can eventually form galaxies (Kaiser 1984; Politzer & Wise 1984; Peacock & Heavens 1985; Bardeen et al. 1986). In the next section, we explicitly assume the volume Γ to be centred on a peak of the underlying smoothed density field. In this case it is possible to take into account *exactly* the correlation between the inertia tensor of the matter contained in Γ and the potential (and hence also density) field. In the following we will still use the notation $\langle \mathbf{L}^2 \rangle_\psi$ to denote the average over the ensemble of realizations of ψ which are compatible with peaks with preselected inertia tensor, $\langle \mathbf{L}^2 \rangle_{\psi|\mathcal{J}}$. The latter corresponds to the average over the (unconstrained) realizations of off-diagonal tidal field (see Appendix B).

2.3 Tidal torques and density peaks

In this subsection, we specialize the ensemble average $\langle \mathbf{L}^2 \rangle_\psi$ to the case in which the volume Γ is centered on a peak of the Gaussian density field. Consequently, the combination of eigenvalues $\mu_1^2 - 3\mu_2$ will depend on the parameters characterizing the peak's shape. The main difficulty to overcome, however, remains that of estimating which fraction of the matter surrounding the primordial peak will eventually collapse onto the peak itself. In other words, the main problem is to estimate the shape of the surface boundary of Γ. This is of course a very difficult and unsolved problem.

Previous analyses of the topology of the constant-density profiles in the neighborhood of the peaks of the Gaussian field δ showed that the isodensity surfaces $\delta_c = \nu_c\sigma_0$, where ν_c is a critical threshold in units of σ_0, are simply connected and approximately ellipsoidal, at least for sufficiently high density peaks (Doroshkevich 1970; Bardeen et al. 1986; Couchman 1987). Hence, we assume that the surface boundary of the volume Γ is determined by the criterion that all the matter above the threshold $\nu_c = 0$ will collapse and form the final galaxy. A similar convention is adopted in Heavens and Peacock (1988).

A density peak is characterised by the conditions of zero gradient, $\nabla\delta = \mathbf{0}$, and negative definite mass tensor $\partial_\alpha\partial_\beta\delta$. The location of the peak is assumed to coincide with the origin $\mathbf{q} = \mathbf{0}$. In the vicinity of the maximum, and in the coordinate system oriented along the principal axes of the mass tensor $\partial_\alpha\partial_\beta\delta$, the density field can be approximated by (Bardeen et al. 1986) $\delta(\mathbf{q}) = \delta(\mathbf{0}) - \frac{1}{2}\sum_\alpha \lambda_\alpha q_\alpha^2$, where λ_α, $\alpha = 1, 2, 3$ are the eigenvalues of the tensor $-\partial_\alpha\partial_\beta\delta$. Since the peak corresponds to a maximum, all λ_α are positive. Furthermore, it can be assumed that, e.g., $\lambda_1 \geq \lambda_2 \geq \lambda_3 > 0$. Expressing the height of the peak in units of σ_0, $\delta(\mathbf{0}) \equiv \nu\sigma_0$, the surface boundary of Γ may now be written as $\sum_\alpha A_\alpha^{-2} q_\alpha^2 = 1$, where the quantities A_α are the principal semi-axes of the ellipsoidal isodensity surface $\delta_c = 0$: $A_\alpha^2 = 2\nu\sigma_0/\lambda_\alpha$. Note that this last relation holds only if $\nu \geq 0$: therefore, all those objects corresponding to local maxima located in regions of below average mean density (void) are not taken into account. Fortunately, such objects will probably fail to form a prominent bound object anyway.

At this point, noting that the inertia tensor $\mathcal{J}_{\alpha\beta}$ is diagonal in the mass tensor eigenframe, and that $\Gamma = \frac{4\pi}{3} A_1 A_2 A_3$, one has (see Appendix B for technical details)

$$\mathcal{L} \equiv \sqrt{\langle \mathbf{L}^2 \rangle_\psi} = \ell\, \mathcal{L}_*\,, \tag{19}$$

where we have defined

$$\mathcal{L}_* \equiv a^2 \dot{D}\, \eta_0\, \sigma_0\, R_*^5\,, \tag{20}$$

and

$$\ell \equiv \frac{96\,\pi}{\sqrt{15^3}}\,(1-\gamma^2)^{1/2}\left(\frac{\nu}{\gamma x}\right)^{5/2}\frac{\mathcal{A}(e,p)^{1/2}}{\mathcal{B}(e,p)^{3/2}}\,. \tag{21}$$

The meaning of the peak shape parameters, whose distribution $\mathcal{P}(\nu, x, e, p)$ is given in Appendix B, is the following. The parameter x is an indicator of the 'sharpness' of the peak, sharper peaks have higher x; the parameters e and p characterize the asymmetry of the isodensity profile: $e \equiv (\lambda_1 - \lambda_3)/2(\lambda_1 + \lambda_2 + \lambda_3)$ and $p \equiv (\lambda_1 - 2\lambda_2 + \lambda_3)/2(\lambda_1 + \lambda_2 + \lambda_3)$. More in detail, the parameter $e(\geq 0)$ measures the *ellipticity* of the matter distribution in the plane (q_1, q_3), while p determines the *oblateness* $(0 \leq p \leq e)$ or the *prolateness* $(-e \leq p \leq 0)$ of the triaxial ellipsoid. If $e = 0$, then $p = 0$, and the ellipsoid is a sphere. The functions $\mathcal{A}(e,p)$ and $\mathcal{B}(e,p)$, which are polynomials in e and p, are given explicitly in Appendix B. For a sphere, $\mathcal{A}(0,0) = 0$ and $\mathcal{B}(0,0) = 1$.

The meaning of the spectral parameters γ and R_* instead is the following. The parameter γ is a measure of the width of the power spectrum: if the spectrum is a delta function, then $\gamma = 1$; on the contrary, if $p^7 P_\psi(p)$ is constant over a wide range of p, then $\gamma \ll 1$; the dependence of γ on scale for a Cold Dark Matter (CDM) power spectrum is displayed in Fig. 1 of Bardeen et al. (1986): typically, $\gamma \approx 0.62$ on galactic scale. The parameter R_* is a measure of the coherence scale of the density field or, in other words, it gives an indication of the smallest wavelength in the power spectrum: R_* is related to the smoothing length R. For a Gaussian filter and a power–law spectrum, $R = \sqrt{(n+5)/6}\,R_*$, where n is the spectral index. To select masses on galactic scale, one typically takes $R \approx 0.5\,h^{-1}$ Mpc (for further details see Bardeen et al. 1986; Appendix B of this paper).

The rms angular momentum $\mathcal{L}$ in equation (19) has been written as a product of two factors. The first factor $\mathcal{L}_* = \mathcal{L}_*(t)$ contains the temporal dependence and can be thought of as the angular momentum unit. On the other hand, the second factor $\ell = \ell(\nu, x, e, p; \gamma)$ is dimensionless and depends explicitly on the peak shape parameters; in addition, ℓ depends on the power spectrum too, through $\gamma^\star$. The unit $\mathcal{L}_*$ and the shape term ℓ are the 'equivalent' of $J_{ref}(t)$ and j_e in equations (10) and (13) in Heavens & Peacock (1988), respectively. (Specifically, $\mathcal{L}_*$ is identical to $J_{ref}(t)$ for $f = 0$, but ℓ is averaged over the constrained field ψ whereas j_e corresponds to one single realisation of ψ, $\ell = \langle j_e^2 \rangle_\psi^{1/2}$.)

The result in equation (19) is quite simple as a consequence of our factoring out of the dependence of angular momentum on the underlying random field ψ on the one hand, and on the peak shape parameters ν, x, e, p on the other hand. This is already manifest in the original equations (13) and (16) and allows a simplification of the calculation of the probability distribution of ℓ, since $\mathcal{P}(\nu, x, e, p)$ and the second moment of the off-diagonal shear components is all we need to know. Heavens & Peacock (1988) calculated the probability distribution function of the modulus $L = |\mathbf{L}|$ of the peak's angular momentum. Since L depends on the shear components, they needed to compute the *joint* distribution of shape parameters ν and λ_α (i.e. ν, x, e and p), and shear field $\mathcal{E}_{\alpha\beta}$; the distribution of early torques on a peak of given height ν then leaves a four dimensional numerical integration. As we will show in Section 3.2, our averaging over the constrained realisations of the gravitational potential narrows only slightly the probability distribution of the angular momentum (see Fig. 7 below).

In the next section, we will compute several distribution functions for different spin parameters: for this purpose it is useful to express the mass $M = \eta_0\,\Gamma$ enclosed by the isodensity ellipsoid in terms of the peak shape parameters:

$$M \equiv m\,M_* = \sqrt{8}\left(\frac{\nu}{\gamma x}\right)^{3/2}\mathcal{B}(e,p)^{-1/2}\,M_*\,, \tag{22}$$

where the reference mass is $M_* \equiv \frac{4\pi}{3}\,\eta_0\,R_*^3$. We stress that the mass of the collapsing object is estimated as the mass within the volume Γ: the filtering procedure, which defines the mass unit M_*, has to be thought of as corresponding to some genuine physical filter (more than an artificial one) which prevents the coupling between the non-linear (small-scale) and the linear (large-scale) modes in the power spectrum of density fluctuations. The term $m(\nu, x, e, p; \gamma)$ describes the deviation (reduction or amplification) of the peak mass with respect to the mass unit M_* in terms of the shape parameters. We now set the smoothing scale $R_* = 0.23\,(0.62/\gamma)^{1/2}\,h^{-1}$ Mpc in order to have $M_* = 1.45\,(0.62/\gamma)^{3/2}\,10^{10}\,h^{-1}\,M_\odot$. This ensures that mean values of M in equation (22) correspond to physical masses $\approx 10^{11} M_\odot$ typical of spiral galaxies and so allows comparison of our angular momentum distributions with galaxy data. To compare against e.g. cluster data, one has to choose an appropriate filtering scale R_*.

It is well known that for individual objects the mass given by (22) is a rather poor estimate of the mass of the final collapsed object, as , e.g., shown by numerical simulations. Indeed, this holds true even for the more sophisticated version of the peak formalism like the excursion set method (see the review in White 1994). Even so, the mass-function predicted by the latter method, the Press-Schechter function, is remarkably close to the measured mass-function. In the same spirit, we

---

★ Actually, the factor $(1-\gamma^2)^{1/2}$ in equation (21) cannot be obtained directly by specializing equation (16) to the case of Gaussian peaks, because it is related to the correlation between inertia tensor $\mathcal{J}$ and the random field ψ, which has been neglected in equation (13) – see Appendix B for a self-consistent derivation. Bearing this in mind, we will continue using the notation $\langle\,\cdot\,\rangle_\psi$, but write the factor $(1-\gamma^2)^{1/2}$ explicitly in the equations that follow.

suggest that the statistical predictions which follow from our adopted procedure are more reliable than the predictions for individual objects.

3 ANGULAR MOMENTUM PROBABILITY DISTRIBUTION FUNCTIONS

In this section we compute the probability distribution of three spin parameters $\ell_\beta \equiv \ell/m^\beta$: (*i*) $\beta = 0$; (*ii*) $\beta = 1$, the specific angular momentum, and (*iii*) $\beta = 5/3$, which is suggested by the dimensional dependence of angular momentum on mass (see below).

The probability distribution of ℓ_β can be computed combining the relation $\ell_\beta = \ell_\beta(\alpha_i)$ with the probability distribution $\mathcal{P}(\alpha_k)$, where the α_k ($k = 1, \ldots, 4$) denote the peak shape parameters. For $\mathcal{P}(\alpha_k)$, we will use the distribution function given by equation (62), appropriate for Gaussian peaks.

A useful statistic is the conditional probability distribution for e.g. ℓ_β, given a specific value of one of the parameters α_k, e.g. given the height of the peak. Such a conditional probability distribution $P(\ell_\beta|\alpha_1)\, d\ell_\beta$ is formally computed from

$$\mathcal{P}(\ell_\beta|\alpha_1)\, d\ell_\beta = C_1 \left(\int d\alpha_3 \int d\alpha_4\, \mathcal{P}(\alpha_k) \left| \frac{\partial \ell_\beta}{\partial \alpha_2} \right|^{-1} \right) d\ell_\beta \,, \tag{23}$$

where C_1 is a normalization constant such that $\int \mathcal{P}(\ell_\beta|\alpha_1)\, d\ell_\beta = 1$. The formal expression (23) is general, but we will usually specialize to the case $\alpha_1 = \nu$ and in Appendix C we will show how to compute the distributions for the different cases $\beta = 0, 1, 5/3$.

The same procedure can be applied to the joint probability distribution of spin ℓ_β and mass m, $\mathcal{P}(m, \ell_\beta)\, dm\, d\ell_\beta$:

$$\mathcal{P}(m, \ell_\beta)\, dm\, d\ell_\beta = \left(\int d\alpha_3 \int d\alpha_4\, \mathcal{P}(\alpha_k) \left| \frac{\partial(m, \ell_\beta)}{\partial(\alpha_1, \alpha_2)} \right|^{-1} \right) dm\, d\ell_\beta \,, \tag{24}$$

where $m(\alpha_k)$ is the mass of the peak in units of M_*. Again, we will show in Appendix C how to specialize the parameters α_k for the different values of β.

3.1 Linear growth era

During the linear growth era, before the peak decouples from the expansion of the Universe, angular momentum ℓ and peak mass m are related to the peak properties through equations (21) and (22) respectively. Noting that ℓ and m depend on ν and x only through the combination $y \equiv \nu/x$, we use equation (24) to obtain:

$$\mathcal{P}(m, \ell_\beta; \nu_1 \leq \nu \leq \nu_2)\, dm\, d\ell_\beta =$$

$$\mathcal{P}_0 \left(\int_0^\infty dy\, \mathcal{W}[e(y, m, \ell_\beta), p(y, m, \ell_\beta)] J_{ep}^{-1} J_{\mathcal{AB}}^{-1} \int_{\nu_1/y}^{\nu_2/y} dx\, x^9\, \exp[-f(y)x^2] \right) dm\, d\ell_\beta \,. \tag{25}$$

This result is obtained by doing the transformation $(e, p) \to (m, \ell_\beta)$ in two steps. Hence, J_{ep} denotes the modulus of the determinant of the transformation $(e, p) \to (\mathcal{A}, \mathcal{B})$ and $J_{\mathcal{AB}}$ is the modulus of the determinant of the Jacobian of the transformation $(\mathcal{A}, \mathcal{B}) \to (m, \ell_\beta)$. The function $f(y)$ appearing in the argument of the exponential follows from equation (62). The integral over the peak sharpness x can be performed analytically, yet the inversion $(\mathcal{A}, \mathcal{B}) \to (e, p)$ cannot, as it involves finding the real roots of a polynomial of degree six! Further technical details can be found in Appendix C.

The last equation is a particular case of equation (24) since $\mathcal{P}(m, \ell_\beta; \nu_1 \leq \nu \leq \nu_2)\, dm\, d\ell_\beta$ is the number of peaks per unit volume, in an interval $dm\, d\ell_\beta$ round specific values m and ℓ_β, which *in addition* have height ν between ν_1 and ν_2. This is because we wish to identify a certain class of objects (e.g., spirals, ellipticals, clusters) assigning a finite ν-interval rather then with a single value of ν (see the discussion in Blumenthal et al. 1984).

The joint distribution of m and ℓ ($\beta = 0$, $\nu_1 = 0$, $\nu_2 = \infty$) is shown in Fig. 1 for $\gamma = 0.62$, typical of the CDM model. Note that the most probable value of ℓ, given m, is strongly correlated with m, causing equiprobability contours to be stretched approximately along $\ell \propto m^{5/3}$. This dependence is obvious on dimensional grounds, since, from Eqs. (20), $\mathcal{L} \propto R_*^5$ and $M \propto R_*^3$, hence $\mathcal{L} \propto M^{5/3}$. It follows that $\mathcal{L}/M^{5/3}$ is independent of the (rather arbitrary) smoothing scale R_* (see the discussion in Heavens & Peacock 1988). This scaling provides an excellent fit to the actual scaling of ℓ with m and is shown in Fig. 1 for comparison.

The joint distribution of m and the specific angular momentum ℓ/m ($\beta = 1$) is shown in Fig. 2, again for $\gamma = 0.62$, for the whole range of ν as well as for restricted ranges, $1/2 \leq \nu \leq 3/2$ and $3/2 \leq \nu \leq 5/2$. We re-iterate that our description of angular momentum for protoobjects is limited to objects with $\nu \geq 0$, hence the *total* number of objects displayed in Fig. 2 is only 96% of the total peak number density for this value of γ i.e., 4% of peaks have $\nu < 0$ for $\gamma = 0.62$. (Note that peaks with $\nu < 0$ are *maxima* in a locally underdense region.) The total number of objects with $1/2 \leq \nu \leq 3/2$ ($3/2 \leq \nu \leq 5/2$) in Fig. 2
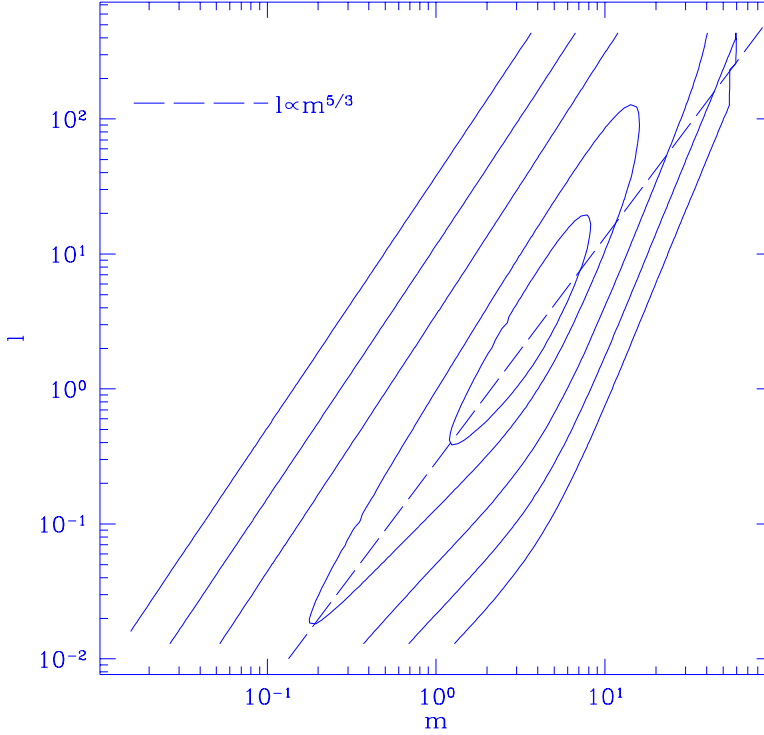
Figure 1. Joint probability distribution $\mathcal{P}(m, \ell)$ for CDM $\gamma = 0.62$. Equiprobability contours are drawn at $\log[m\,\ell\,\mathcal{P}(m, \ell)\ln(10.)^2] = -9, -7, -5, -3, -2$. The scaling $\ell \propto m^{5/3}$ is indicated by the dashed line.

is 40.1% (37.5%) of the total number of objects shown. The equiprobability contours for peaks with the shown restrictions on ν display a steeper dependence, $\ell \propto m^{8/3}$, however, the most probable ℓ versus most probable m, averaged over ν, again scales as $\ell_{\rm mp} \propto m_{\rm mp}^{5/3}$. The figure also shows that objects with the larger value of ν tend to be more massive and in addition have a slightly larger ℓ/m as well.

The dependence on peak height ν is further illustrated in Fig. 3 which shows the joint probability distribution $\mathcal{P}(m, \ell_{\frac{5}{3}})$, which, in view of the strong dependence $\ell \propto m^{5/3}$, is the more appropriate quantity to graph. Note that the most probable value of $l/m^{5/3}$ is very insensitive to ν, however, the *dispersion* round the mean is large.

Conditional probability distributions for ℓ and m for given peak height ν are shown in Figs. 4 and 5, which also illustrate the effect of the spectral parameter γ. Higher ν peaks have a higher median ℓ. This effect is stronger for lower γ yet the distributions are very wide, as was found previously by Heavens & Peacock (1988) though for the distribution of the modulus of the angular momentum.

Figure 5 shows the distribution of masses, given ν. In contrast to Fig. 4, we have normalised this distribution to $\int \mathcal{P}(m|\nu) \, dm \, d\nu = 0.016/R_*^3$, to illustrate the different number of objects of given ν, in addition to the distribution as a function of mass. Again distributions are wide, with number of objects falling to 1% of the peak value for masses differing by factors of five either side of the mean mass.

So far we have restricted ourselves to the growth of the angular momentum in the linear regime. However, this era of growth is not generally prone to comparison with observations (but it can be compared against numerical simulations!) since observed structures (galaxies, clusters) have already collapsed. Fortunately, objects presumably acquire most of their angular momentum before they collapse, since tidal torques are much less effective afterwards (Peebles 1969, Catelan & Theuns 1996). However, the non-linear processes during collapse lead to a redistribution of angular momentum over the different subunits that will make up the *final* object in a complicated way (White 1984; Barnes & Efstathiou 1987; Frenk 1987).

We will follow Peebles (1969) in assuming that the linear growth effectively ceases after maximum expansion of the object and identify the angular momentum at that time with the 'final' angular momentum. This might be a partial description of reality.
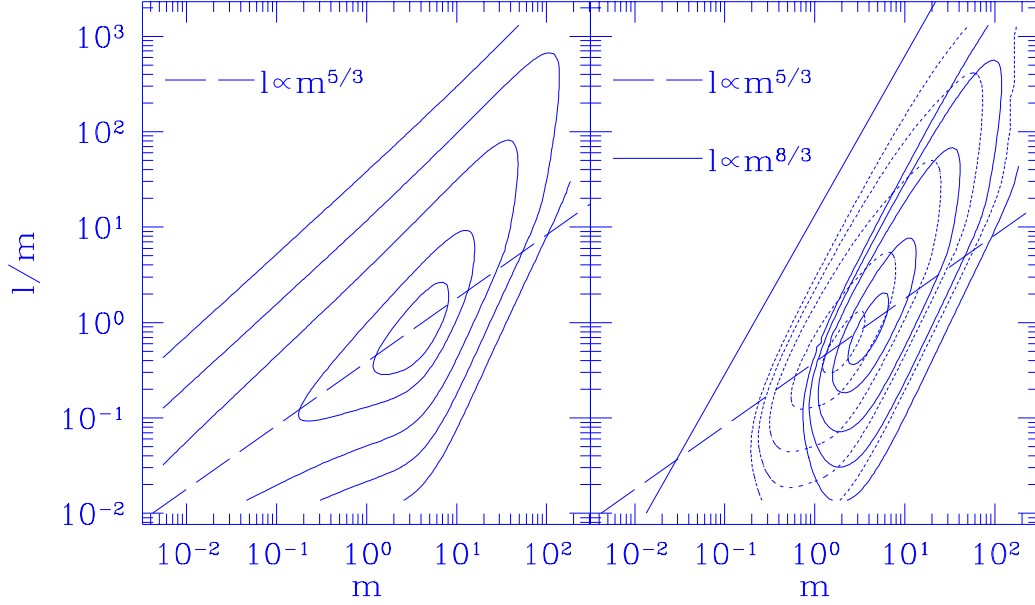
Figure 2. Same as Fig. 1, but for the specific angular momentum ℓ/m. Left: equiprobability contours for all objects with $\nu \geq 0$. Right: dotted equiprobability contours correspond to objects with $1/2 \leq \nu \leq 3/2$ and continuous contours to objects $3/2 \leq \nu \leq 5/2$. Scalings $\ell \propto m^{5/3}$ and $l \propto m^{8/3}$ are indicated.

3.2 Spin distributions at maximum expansion time

Let us assume that the angular momentum growth described by the equation (7) stops as the protogalaxy separates from the overall expansion and collapses back onto itself. A fiducial final angular momentum $\mathbf{L}_f$ (i.e. $\mathcal{L}_f$) can be calculated as the value of $\mathbf{L}$ at the time t_M when, say, $\delta(M) = -D(t_M)\nabla^2\psi \equiv -D_M\nabla^2\psi = 1$. From equation (7) and denoting the mass and radius of the collapsing object by M and R respectively, we get:

$$L_f \sim a_M^2 \dot{D}_M \nabla^2\psi \, MR^2 = a_M^2 \frac{\dot{D}_M}{D_M} MR^2 \propto \frac{\dot{D}_M}{D_M} \rho_{bM}^{-2/3} M^{5/3} \propto \frac{\dot{D}_M}{D_M}\left(\frac{\dot{a}_M}{a_M}\right)^{-4/3} M^{5/3} \; . \tag{26}$$

Since in the Einstein-de Sitter universe $a \propto D \propto t^{2/3}$, the previous result simplifies to (White 1994)

$$L_f = L(t_M) \propto M^{5/3} \, t_M^{1/3} \; . \tag{27}$$

This expression will be useful when analysing the dimensionless spin parameter in the next section. Note that, since t_M depends on M, the latter equation does *not* imply that $t_M^{1/3}$ is the full temporal dependence of L_f on t_M – see below. (In a more general Friedman model, an additional dependence on the density parameter Ω appears, which is approximately a scaling $L_f \propto \Omega^{-0.07}$. Hereafter we will limit ourselves to the EdS case.)

In the case M refers to the mass of a peak of height ν, the maximum expansion time t_M depends implicitly on ν, which we emphasize by writing $t_M \equiv t_{M(\nu)} \equiv t_\nu$. The scaling of t_ν with ν may be recovered extrapolating the linear spherical model to the maximum expansion time, giving $t_\nu = \nu^{-3/2} t_{\nu=1}$. From equation (20) we find that the 'final' ensemble averaged angular momentum contains an extra dependence $\mathcal{L}_f \propto \nu^{-3/2}$ on peak height in comparison to the linear $\mathcal{L}$:

$$\mathcal{L}_f(t_\nu) = \ell \, \mathcal{L}_*(t_\nu) = \ell \, \nu^{-3/2} \, \mathcal{L}_*(t_{\nu=1}) \equiv \ell_f \mathcal{L}_*(t_{\nu=1}) \; . \tag{28}$$

The argument goes as follows: start from equation (20) for the unit of spin $\mathcal{L}_*$, which we want to compute at the maximum expansion time (defined by $\nu D(t_\nu)\sigma_0 \equiv \nu D_\nu \sigma_0 = 1$ for a perturbation of height ν):

$$\mathcal{L}_*(t_\nu) = a_\nu^2 \dot{D}_\nu \, \eta_0 \sigma_0 R_*^5 = \frac{a_\nu^2 \dot{D}_\nu}{\nu D_\nu} \eta_0(\nu D_\nu \sigma_0)R_*^5 = \frac{a_\nu^2 \dot{D}_\nu}{\nu D_\nu} \eta_0 \, R_*^5 \; . \tag{29}$$

Consequently, since $a_\nu^2 \dot{D}_\nu / D_\nu \propto t_\nu^{1/3}$ in the EdS universe,

$$\mathcal{L}_*(t_\nu) = \nu^{-1} \, t_\nu^{1/3} \eta_0 R_*^5 \propto t_\nu \; . \tag{30}$$
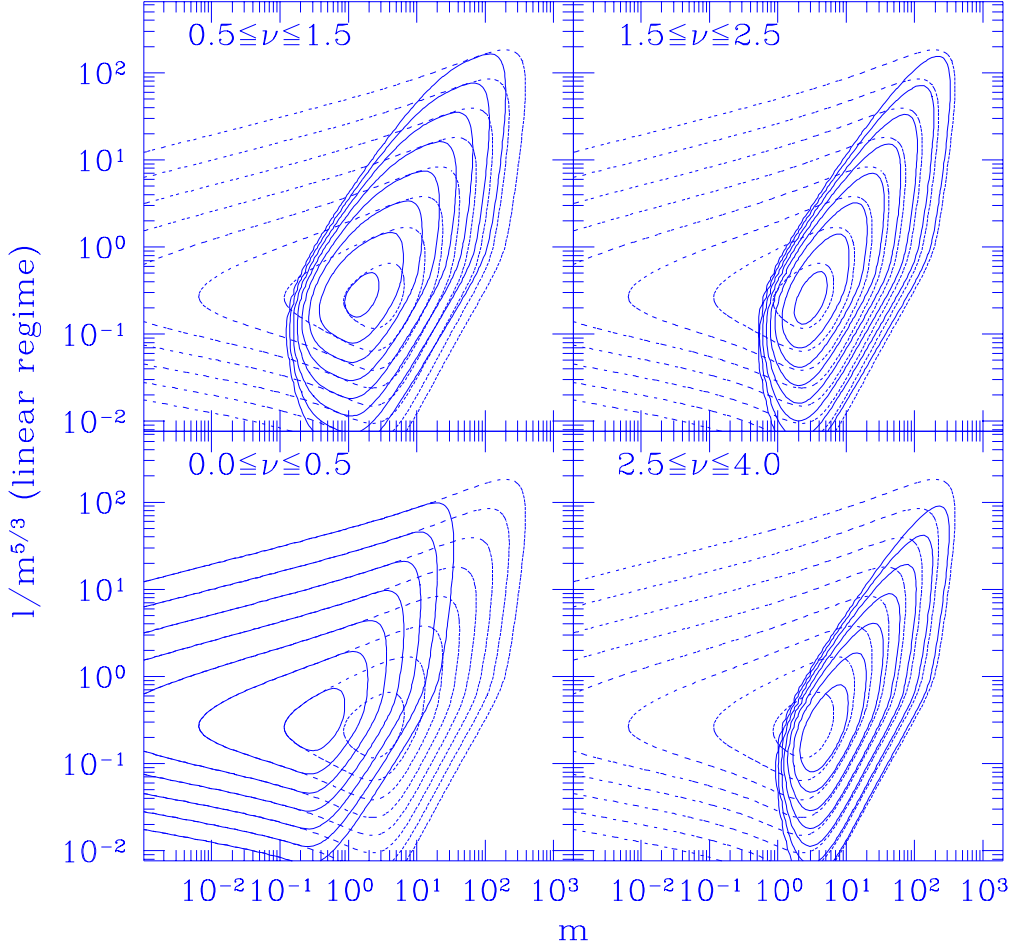
Figure 3. Joint probability distributions $\mathcal{P}(m, \ell_{\frac{5}{3}}; \nu_1 \leq \nu \leq \nu_2)$ for CDM $\gamma = 0.62$. Equiprobability contours are drawn at $\log[m \, \ell_{\frac{5}{3}} \, \mathcal{P}(m, \ell_{\frac{5}{3}}; \nu_1 \leq \nu \leq \nu_2) \ln(10.)^2] = -9, \ldots, -3, -2$. Different panels correspond to different ranges $[\nu_1, \nu_2]$, as indicated. The dotted contours are identical in all panels and correspond to the whole range $[\nu_1 = 0, \nu_2 = \infty)$.

Evaluating this for $\nu = 1$ gives the expression $(28)^{\dagger}$. Explicitly, $\mathcal{L}_*(t_{\nu=1})$ is calculated at the time of maximum expansion of a spherical $\nu = 1$ overdensity, $D(t_{\nu=1})\sigma_0 = (3/20)(6\pi)^{2/3}$:

$$
\begin{aligned}
\mathcal{L}_*(t_{\nu=1}) &= a^2 \dot{D} \eta_0 \sigma_0 R_*^5 \big|_{t=t_1} = \frac{9(6\pi)^{2/3}}{160\pi} G^{-1} R_*^5 \left(a^5 H^3\right)_{t=t_1} = \frac{9(6\pi)^{2/3}}{160\pi} G^{-1} H_0^3 (1+z)_{t=t_1}^{-1/2} R_*^5 \\
&= 2.4 \times 10^{66} \left(\frac{h}{0.5}\right)^{-2} \left(\frac{1+z}{4}\right)_{t=t_1}^{-1/2} \left(\frac{M_*}{1.45 \times 10^{10} h^{-1} M_\odot}\right)^{5/3} \ \text{kg m}^2 \ \text{s}^{-1} \\
&= 1362 \left(\frac{h}{0.5}\right)^{-1} \left(\frac{1+z}{4}\right)_{t=t_1}^{-1/2} M_* \left(\frac{M_*}{1.45 \times 10^{10} h^{-1} M_\odot}\right)^{2/3} \ \text{km s}^{-1} \, \text{kpc} \ .
\end{aligned}
\tag{31}
$$

Here, H is the Hubble constant, $H_0 = 100 \, h$ km/s/Mpc is the present day Hubble constant, z is the redshift. On the other hand, ℓ_f is given by

$$
\ell_f \equiv \nu^{-3/2} \, \ell = \frac{96 \, \pi}{\sqrt{15^3}} \, (1 - \gamma^2)^{1/2} \, \nu^{-3/2} \, \left(\frac{\nu}{\gamma x}\right)^{5/2} \frac{\mathcal{A}(e,p)^{1/2}}{\mathcal{B}(e,p)^{3/2}} \ .
\tag{32}
$$

† The same scaling $L_f \propto \nu^{-1} M^{5/3} t_M^{1/3}$ for the modulus of the angular momentum may be recovered directly from the dimensional analysis in equation (26), but remembering that $(\alpha \neq \beta) \ L_f \sim \partial_\alpha \partial_\beta \psi \sim \nu^{-1} \nabla^2 \psi$; we recall that the off-diagonal elements of the shear tensor are *independent* of ν while the trace $\nabla^2 \psi$ is proportional to ν.
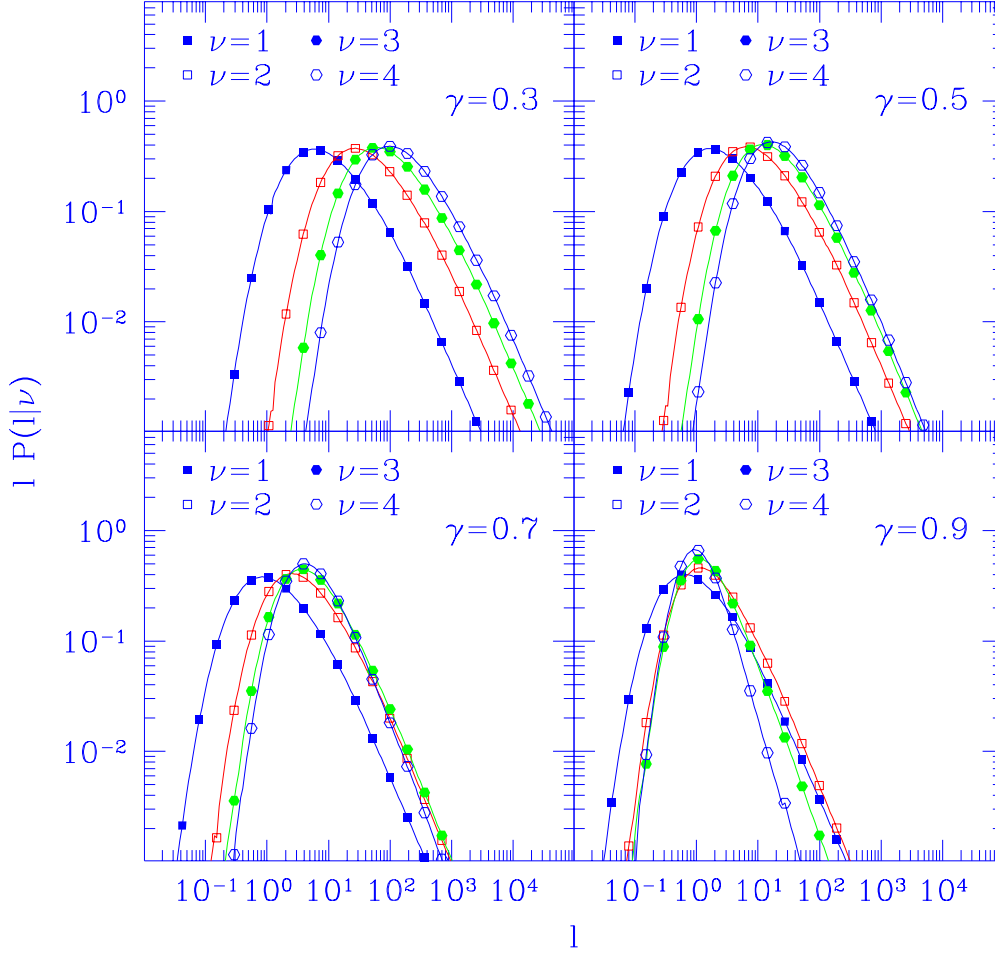
Figure 4. Conditional probability for angular momentum ℓ during the linear regime, given the peak height ν, for different values of the spectral parameter γ. Different symbols denote different values of ν, as indicated in the figure. These plots can be compared against the corresponding ones in Fig. 1 in Heavens & Peacock (1988) – see the discussion in the text.

The first equality can be compared with equation (16) in Heavens & Peacock (1988), which exhibits the same scaling $\nu^{-3/2}$.

Figure 6 illustrates the dependence of $\ell_f/m^{5/3}$ at maximum expansion as a function of m for several values of the spectral parameter γ. In all cases, equiprobability contours are elongated along $\ell_f/m^{5/3} \propto m^{-1}$, a scaling which follows from the $\ell_f \propto \nu$ dependence read from equation (32) and the dependence $m \propto \nu^{3/2}$, from equation (22). Note that the higher γ distributions are significantly more peaked round their maximum.

The conditional probability of final angular momentum ℓ_f for peaks of given height ν is plotted in Fig. 7 for several values of the spectral parameter γ. Superposed is the corresponding curve (for $\gamma = 0.5$) of Heavens & Peacock (1988). The comparison is complicated by the fact that we are plotting in the same diagram the probability distribution for two different quantities, essentially $\mathcal{P}(L_f/\mathcal{L}_*|\nu)$ for the modulus of the angular momentum and $\mathcal{P}(\langle \mathbf{L}_f^2 \rangle_\psi^{1/2}/\mathcal{L}_*|\nu)$ for the rms angular momentum. This introduces a very small shift between the median values of $|\mathbf{L}_f|$ and $\langle \mathbf{L}_f^2 \rangle_\psi^{1/2}$ which we estimate by computing the ratio $\chi \equiv \langle \mathbf{L}_f^2 \rangle^{1/2}/\langle |\mathbf{L}_f| \rangle$. In the case of a rotationally symmetric ellipsoid, with $\mathcal{J}_{11} = \mathcal{J}_{22}$, we find that $\chi = \langle \mathcal{D}_{13}^2 + \mathcal{D}_{23}^2 \rangle^{1/2}/\langle (\mathcal{D}_{13}^2 + \mathcal{D}_{23}^2)^{1/2} \rangle = \sqrt{4/\pi} \approx 1.13$, using the fact that $\mathcal{D}_{\alpha\beta}$ is Gaussian distributed with variance $\sigma_0^2 (1-\gamma^2)/15$. As Fig. (7) testifies, the distribution of $\mathcal{L}_f$ is slightly narrower than that of L_f (because of the shear averaging already performed) but is still very broad; we stress that the two spin distributions agree extremely well for medium and large values of the angular momentum. From this we conclude that the rms angular momentum $\mathcal{L}_f$ is a good estimator for L_f and that the loss of information, caused by averaging over the constrained realisations of the field, appears to be small. These results are useful when discussing the galaxy morphology versus rotational properties.
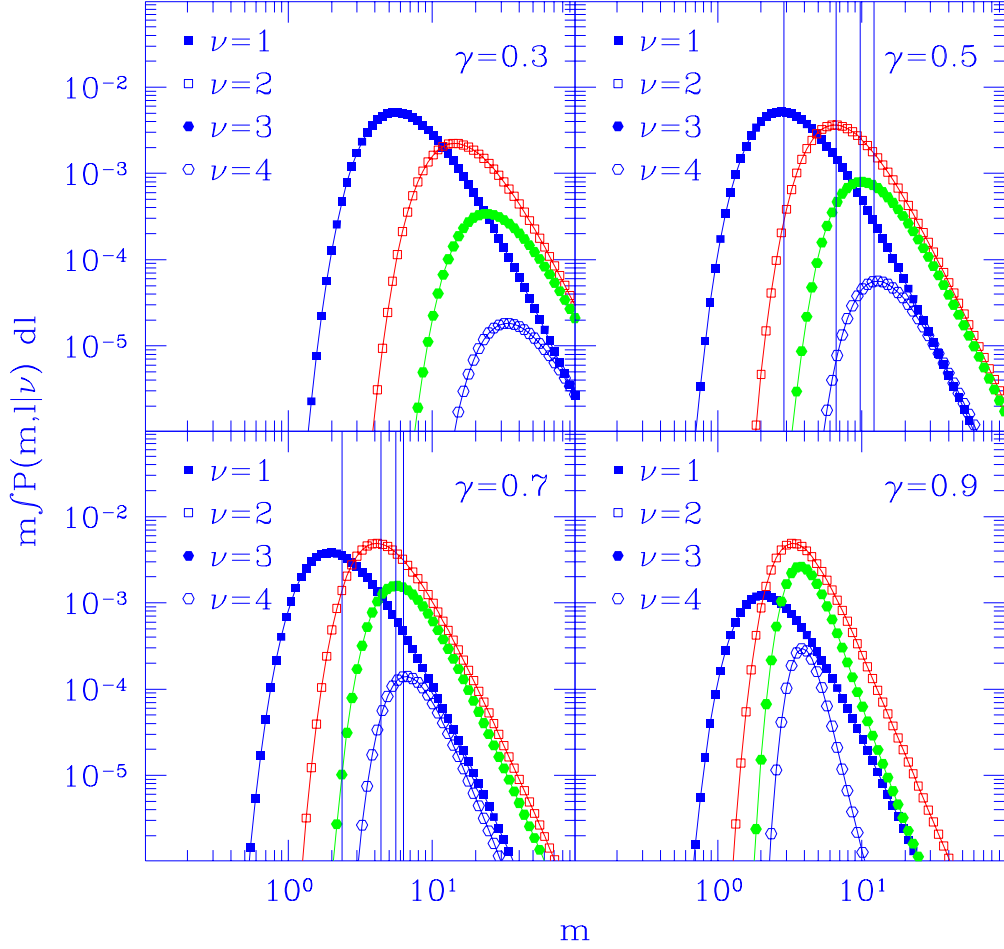
Figure 5. Distribution of mass for peaks of given height, for several values of the spectral parameter γ. Unlike Fig. 4, mass probabilities shown here are not normalised to one, but reflect the fact that there are fewer peaks of higher ν. Vertical lines in panels $\gamma = 0.5$ and $\gamma = 0.7$ denote the values of the most probable mass, given ν, obtained from Peacock & Heavens (1990) which fit well. Different symbols denote different values of ν, as indicated in the figure.

4 GALAXY MORPHOLOGY AND ANGULAR MOMENTUM

In this section we compare our predictions against observational data on both the dimensionless spin parameter λ and the specific angular momentum L/M.

4.1 Dimensionless spin parameter

A conventional parametrization of galactic angular momenta is the dimensionless spin parameter λ

$$\lambda \equiv L\,|E|^{1/2}\,G^{-1/2}\,M^{-5/2} \,, \tag{33}$$

which is a measure of the ratio between the observed angular velocity ω and the angular velocity ω_0 which would be required to support the system centrifugally (such as e.g. a rotationally supported self-gravitating disc): $\lambda \approx \omega/\omega_0 \approx [L/(M\,R^2)]/[(GM/R^3)^{1/2}]$, where L is the modulus of the angular momentum, E is the total binding energy of the pro-toobject.

Typically, λ depends on the galactic morphological type, being as high as $\lambda \approx 0.5$ for spirals and S0 galaxies, but only $\lambda \approx 0.05$ for ellipticals, although the dispersion around these values is large [Efstathiou & Jones 1979; Fall & Efstathiou 1980; Kashlinsky 1982; Fall 1983; Davies et al. 1983, Efstathiou & Barnes 1984. More in detail, bright giant ellipticals (magnitude $M_B < -19$) rotate more slowly than faint ellipticals ($M_B > -19$), and the latter are observed to rotate nearly as rapidly as bulges of spirals and lenticulars of the same luminosities (Kormendy & Illingworth 1982; Illingworth & Schechter 1982).
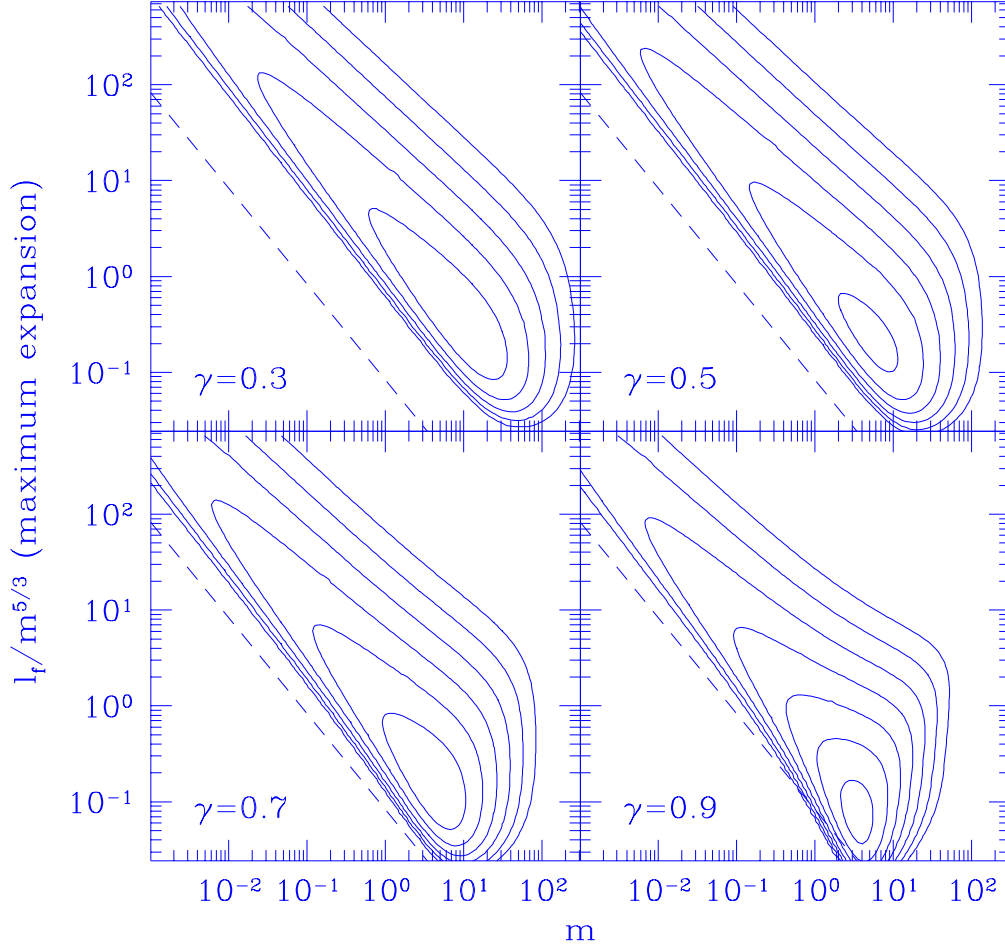
Figure 6. Joint probability distribution $\mathcal{P}(m, \ell_{\frac{5}{3}, f})$, where $\ell_{\frac{5}{3}, f} \equiv \ell_f / m^{5/3}$, at maximum expansion time for different values of the spectral parameter γ. Equiprobability contours are drawn at $\log[m\, \ell_{\frac{5}{3}, f}\, \mathcal{P}(m, \ell_{\frac{5}{3}, f})\, \ln(10.)^2] = -9, \ldots, -3, -2$. The dashed line in each panel is the same and indicates the scaling $\ell_{\frac{5}{3}, f} \propto m^{-1}$.

Also, the flattening of giant ellipticals is thought to be due to velocity anisotropy rather than to coherent rotation (Binney 1978)]. We will re-examine below the question of the correlation between the galaxy morphology and the amount of angular momentum.

A theoretical estimate of λ may be determined from its ensemble average, $\Lambda \equiv \sqrt{\langle \lambda^2 \rangle_\psi}$. From equation (33), one immediately obtains

$$\Lambda \equiv \mathcal{L}\, |E|^{1/2}\, G^{-1/2}\, M^{-5/2} \,, \tag{34}$$

where we have assumed that the total energy E is the *same* for any realisation of the potential field ψ (i.e. it is independent of the deformation tensor $\mathcal{D}_{\alpha\beta}$). This is of course a questionable assumption. It is well known how difficult in general is the exact calculation of E for a generic enclosing volume Γ. Hoffman (1988), expanding the total energy to first order in δ, the gravitational potential to second order in the position and assuming an ellipsoidal isodensity boundary for Γ, obtained an expression for E in terms of the deformation tensor, $E \propto \mathcal{D}_{\alpha\beta}\mathcal{J}_{\alpha\beta}$. Such a dependence on the deformation tensor of E, when consistently taken into account, would hugely complicate the calculation of Λ.

However, the *order of magnitude* of the total energy may be quantified applying the spherical top-hat model to the evolution of the overdensity contained in Γ (see, e.g., Peebles 1980): we expect that such a model becomes a better approximation as the height of the peak increases, since high-ν peaks tend to be more spherical. The spherical model is adopted for the same purpose in Heavens & Peacock (1988).
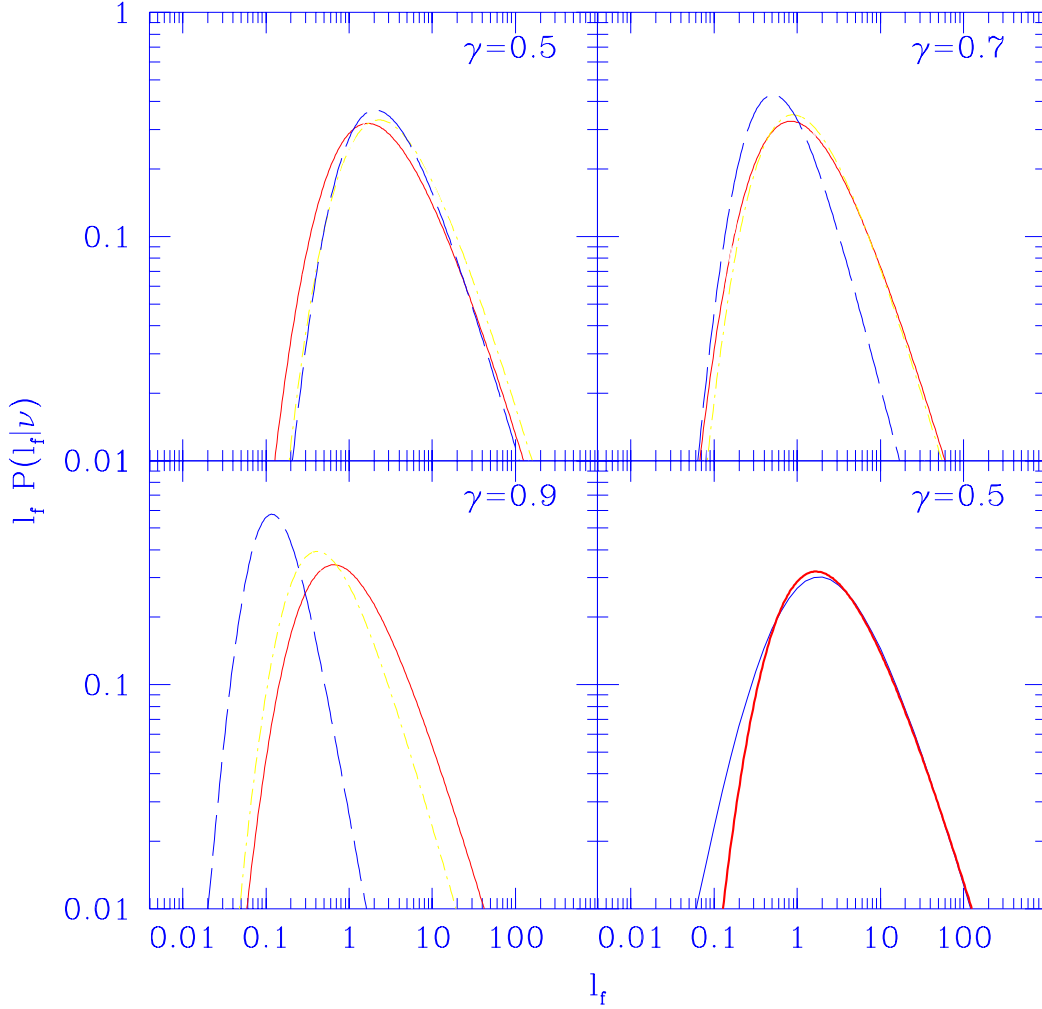
Figure 7. Conditional probability distribution for final angular momentum ℓ_f given the peak height ν for several values of the spectral parameter γ. Continuous lines: $\nu = 1$, dot-short dashed: $\nu = 2$, short dashed: $\nu = 3$, long dashed: $\nu = 4$, for $\gamma = 0.5$, 0.7 and 0.9. Lower right panel ($\gamma = 0.5$), a comparison against the Heavens & Peacock distribution is shown (see discussion in text). Thick line: distribution for $\nu = 1$; thin line: fit for $\nu = 1$ of the distribution shown in Figure 2a of Heavens & Peacock (1988),$\mathcal{P}(\ell_f | \nu = 1) = 8.2/[(0.89/\ell_f)^{0.25} + (\ell_f/0.89)^{0.47}]^5$. Note the excellent agreement between these two distributions for medium and large values of the angular momentum.

Since the total binding energy of the protogalaxy scales with maximum expansion time as $E \propto M^{5/3} t_M^{-2/3}$, then equation (27) implies that the *final* spin parameter λ_f (or, equivalently, Λ_f) does *not* depend on the collapse time t_M (actually, this should hold provided that the protoobject is isolated from the rest of the universe and that dissipation processes are negligible during the linear evolution).

The resulting expression for the final spin parameter Λ_f depends on the peak shape parameters as follows

$$\Lambda_f = \frac{27\,\pi}{250}\,(1 - \gamma^2)^{1/2}\,\nu^{-1}\,\frac{\mathcal{A}(e,p)^{1/2}}{\mathcal{B}(e,p)^{2/3}}\;, \tag{35}$$

where, in the framework of the spherical model, the expression for the matter density of the protogalaxy at the maximum expansion time $t_{M(\nu)} = t_\nu$, $\rho(t_\nu) = (3\pi/4)^2 \rho_b(t_\nu)$, and the linear prediction of the root mean square density field, $D(t_\nu)\sigma_0 = (3/20)(6\pi)^{2/3}\nu^{-1}$, have been used. An analogous expression for Λ_f, in terms of the quantity $\ell_{\frac{5}{3},f}$ discussed in the previous section, is

$$\Lambda_f = \sqrt{\frac{(3/2)^9}{500}}\,\nu^{1/2}\,\ell_{\frac{5}{3},f}\;, \tag{36}$$

which can be compared against equation (28) in Heavens & Peacock (1988). Note that their equation (28) for λ_f corresponds to a single realisation of ψ (but recall that their probability function for λ_f does take the shear distribution into account);
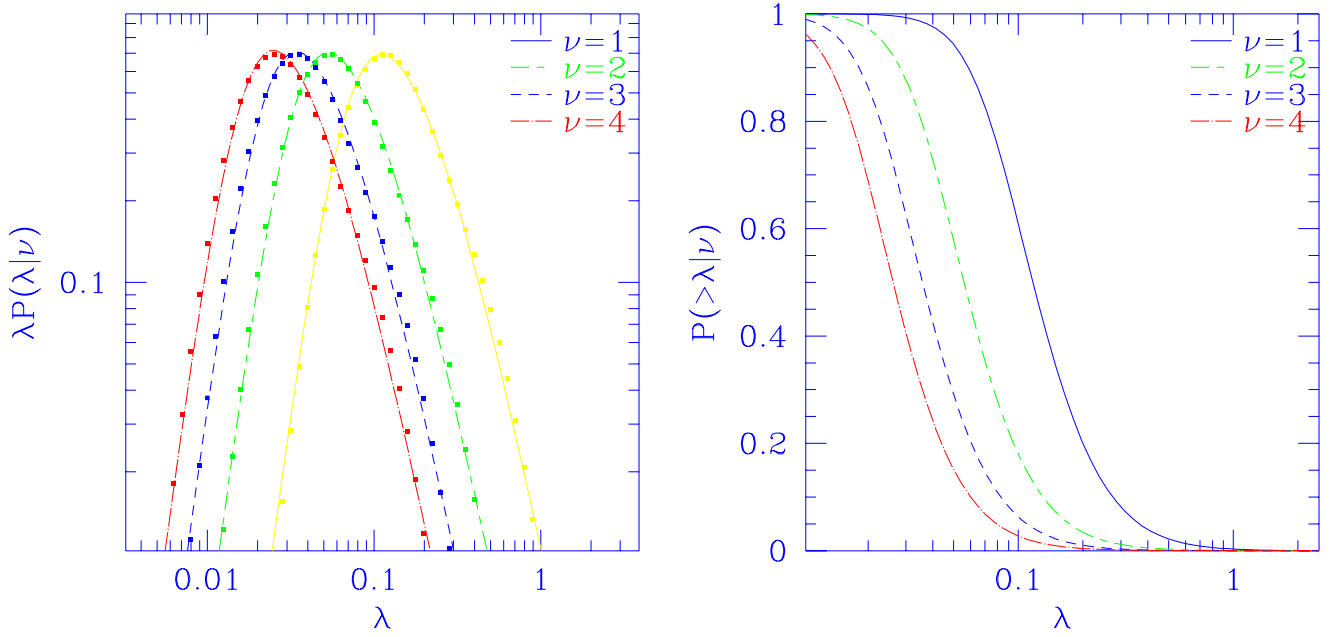
Figure 8. Left panel: curves denote the conditional probability distributions for λ for different peak heights ν for a CDM spectrum ($\gamma = 0.62$). The squares correspond to the fit given in equation (37). Right panel: cumulative distributions for λ for the same ν and γ.

however the scaling $\lambda_f \propto \nu^{-1}$ obtained here is the same: indeed, starting from their definition (19) of $j_{\frac{5}{3}}$, one finds the scaling $j_{\frac{5}{3}} \propto \nu^{-3/2}$ from which one recovers the scaling $\lambda_f \propto \nu^{-1}$ in their equation (28). The underlying reason for this is that the ensemble average over the shear does not introduce a ν dependence.

Recently, Steinmetz and Bartelmann (1995) attempted to analyze the λ parameter in terms of the peak shape parameters (note that their definitions of e and p are different from ours). Unfortunately, their statistical analysis is rather crude since they do not compute the probability distribution of their e and p and hence are unable to perform the proper average $\langle \lambda^2 \rangle^{1/2}$ (compare their equations (44) and (56)).

The probability distribution function $\mathcal{P}(\Lambda_f|\nu)$, obtained from equation (35), is displayed in Fig.8 and can be compared against Fig. 4 in Heavens & Peacock (1988), bearing in mind that our plots are for the rms spin parameter. Although these authors do not show the case $\gamma = 0.62$, $\gamma = 0.7$ is sufficiently close to the CDM value to allow a direct comparison.

The fit shown in Fig. 8 is

$$\Lambda_f \mathcal{P}(\Lambda_f|\nu) \approx \mathcal{F}_0 \left[1 + \alpha \left(\frac{\Lambda_f}{\Lambda_0(\nu)} \right)^4 \right] \exp \left[-\frac{\log^2 \left(\frac{\Lambda_f}{\Lambda_0(\nu)} \right)}{2 \log \Theta} \right] , \qquad (37)$$

where $\mathcal{F}_0 = 0.68$, $\alpha = 0.02$, $\Theta = 1.12$ and $\Lambda_0(\nu) = 0.11 \, \nu^{-1.1}$. This fits the actual distribution well for $\nu = 1 - 4$. Note that the median $\overline{\Lambda}_f \approx \Lambda_0(\nu)$ has a slightly steeper dependence on ν than expected from equation (35). (In Fig. 8 we used the symbol λ for Λ_f.)

It can be seen from Fig.8 that higher ν-peaks have on average lower final angular momentum Λ_f: such a statistical anti-correlation between Λ_f (i.e. λ_f) and the peak height ν has been first found by Hoffman (1986; 1988) and Heavens & Peacock (1988). We also confirm that the Λ_f–distributions are very broad (factor ~ 10), and the shift between curves of different λ is small in comparison with the width of the distribution. Consequently, a given value of λ cannot be unambiguously identified with a specific value of ν.

We stress the fact that the curve corresponding to $\mathcal{P}(\Lambda_f|\nu = 1)$ has the median value $\overline{\Lambda}_f = \int d\Lambda_f \, \Lambda_f \, \mathcal{P}(\Lambda_f|\nu = 1) = 0.15$. This brings the value for the Λ_f for the halos of the progenitors of spiral galaxies, if assumed to coincide with $\nu = 1$ primordial peaks on galactic scales (Blumenthal et al. 1984), within a factor of two of the spin parameter of the luminous parts of observed spirals.

It has often been said that energy dissipating cooling processes are necessary to explain the high spin values of spiral galaxies (e.g. Efstathiou & Jones 1979; Fall & Efstathiou 1980), and dissipationless N-body simulations produce objects with

$\lambda \sim 0.08$, too low for spiral galaxies (Barnes & Efstathiou 1987). However, newer N-body simulations which include dissipation (e.g. Navarro, Frenk & White 1995) still fail to produce objects with high λ.

If our method for describing tidal torques is sound, then the importance of cooling processes to boost the value of λ from the values found from dissipationless N-body calculations $\lambda \approx 0.08$ to values $\lambda \approx 0.5$ found for observed spirals might be partially relaxed. Although we understand that cooling must be important to explain why the luminous matter of galaxies is concentrated in the middle of the dark halos, it should not be invoked as the only cause of the increment of λ for spirals with respect to the one for ellipticals, it could be partially explained on statistical grounds. [Furthermore, we estimate (Catelan & Theuns 1996) that the inclusion of mildly non-linear leading-order corrections to **L** increases the value of λ over that of the purely linear prediction by a factor ≈ 1.3.]

Our analysis supports the suggestion that, in hierarchical clustering scenarios, the higher ν fluctuations will originate rather smaller λ values, the $\nu \sim 1$ fluctuations on galactic scale being statistically associated with spiral galaxies and higher ν fluctuations with ellipticals (Sandage, Freeman & Stokes 1970; Kashlinsky 1982; Faber 1982; Blumenthal et al. 1984; Hoffman 1988).

However it is important to recall that our estimate of Λ_f is based on an extrapolation of the linear theory and, as discussed in Barnes & Efstathiou (1987) and White (1984; 1994), the linear angular momentum is a relatively poor indicator of the final angular momentum of a *highly* non-linear clump of matter ($\sigma \gg 1$). Non-linear dynamical effects (outward/inward convective motion of matter etc.), observed to operate in N-body simulations, tend to *reduce* by a factor ~ 3 the final value of L from the extrapolation of linear theory [although the total scatter about the mean relation is also a factor of ~ 3: see the discussion in Barnes & Efstathiou (1987)]. Clearly, one cannot hope to describe such highly non-linear effects in an exact analytical way.

4.2 Specific angular momentum

An obvious advantage of studying the specific angular momentum L/M, rather than the dimensionless parameter λ, is that the first does not depend on the binding energy E and therefore is not affected by uncertainties associated with dissipative processes. In addition, L/M is not plagued by the problem of how to compute (analytically) or measure (observationally or from N-body simulations) the energy of the object. Consequently, L/M is a more robust estimator of the angular momentum of an object and is better suited to compare different methods of obtaining L. (In view of the strong dependence $L \propto M^{5/3}$, the ratio $L/M^{5/3}$ would be an even better discriminant.)

A comparison of our predictions on L/M against observations is made possible by the data presented in Fig. 1 of Fall (1983), who gives values of M (luminous) and L/M for a set of elliptical, Sb and Sc galaxies. This figure shows that the visible parts of the sampled spiral galaxies have about 6 times as much angular momentum as elliptical galaxies of the same mass. In Fig. 9 we superimpose the data of Fall (1983) on equiprobability contours of $\mathcal{P}(M, \mathcal{L}_f/M)$ obtained by translating to physical units the probability distribution $\mathcal{P}(m, \ell_{1,f})$, with $\ell_{1,f} \equiv \ell_f/m$, calculated in the previous section. We stress that Fall's masses refer to the luminous parts of the galaxies and so should be converted to total masses to allow a comparison. Unfortunately, this procedure is not well defined and we have computed the required scaling factor as $\sqrt{2}/\lambda$, as suggested in Fall (1983) for spirals. Taking $\lambda = 0.15$ for spirals and $\lambda = 0.07$ for ellipticals, as suggested by our analysis for $\nu \approx 1$ and $\nu \approx 2$, we find factors 9.4 and 20, respectively. The smoothing scale is chosen such that the median mass corresponds to the typical mass of a spiral galaxy. The agreement between the maximum probability contour and the location of spiral galaxies is rather remarkable. However, it is clear from the figure that our prediction of $\mathcal{L}_f/M$ does not fully accommodate the data of ellipticals which tend to fall outside high probability contours (but see the discussion in the last subsection), yet more definite conclusions cannot be drawn because of the evident smallness of the sample. A larger sample of data would enhance the fairness of the comparison. The right panel shows equiprobability contours for objects with a restricted range in peak height. The location of spiral galaxies is fitted well when selecting peaks with $\nu \approx 1$. Selecting peaks with $\nu \approx 2$ does tend to shift contours towards the zone occupied by ellipticals, yet falls short of obtaining good agreement. On the whole, it does appear that within our description it is not possible to discriminate between the rotational properties of spirals and ellipticals *solely* on the basis of the initial peak height ν.

It is well known that there is a strong correlation between galaxy type and environment, in the sense that ellipticals tend to occur in regions of high galaxy density while spirals tend to avoid such regions. Hence, interactions between galactic systems, either in the proto or in the collapsed stages, have an influence on the properties of the final observed structures. However, even if it were true that ellipticals form from $\nu \approx 2$ peaks, and although it is well known that, within the peaks formalism, higher ν-peaks are naturally clustered more strongly, the likely direct effects of such enhanced clustering on the *tidal torques* on the peaks themselves are not completely taken into account here. This is best illustrated recalling the fact that the off-diagonal shear components are *independent* of ν, or, in other words, the (off-diagonal part of the) shear field does not take into account the effect of the stronger clustering of higher peaks. So one is possibly missing one of the most basic ingredients which might generate different types of galaxies. Consequently, it is likely that elliptical galaxies are not well described by our formalism. We suggest that, with regard to this matter, the model might be improved by extending the Taylor expansion – which led to equation (7) – to higher order.
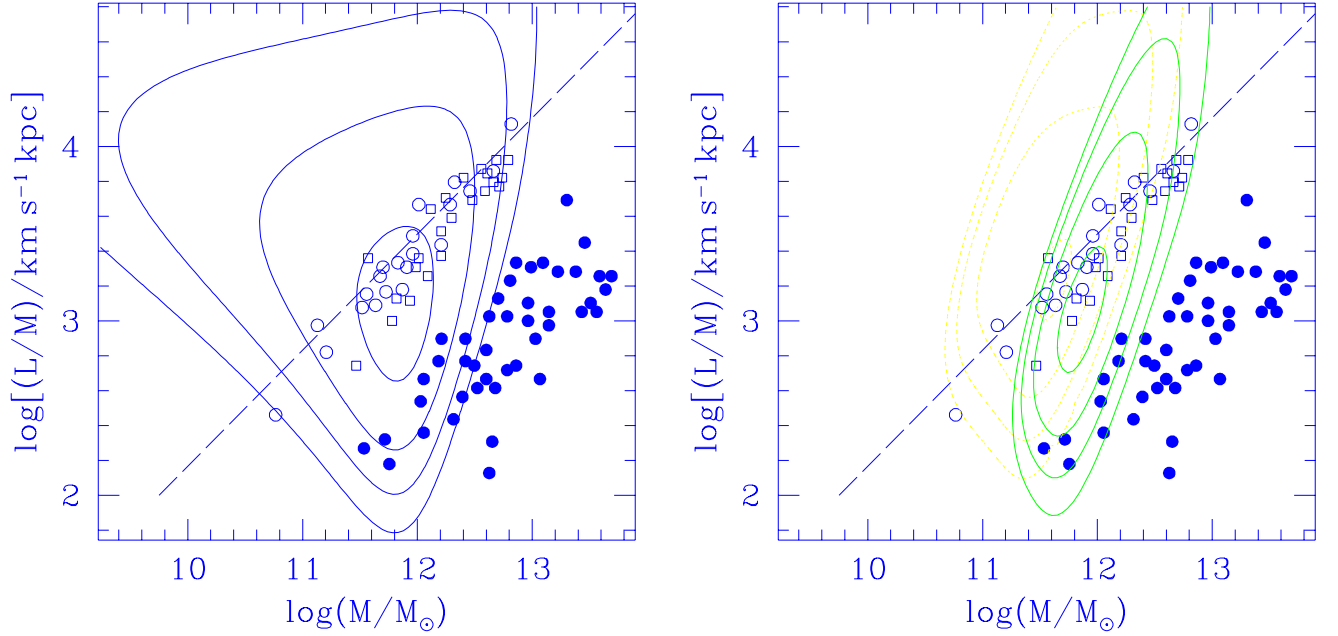
Figure 9. Symbols: observational data as taken from Fall (1983); •: ellipticals, □: Sb and ○: Sc. Luminous masses from Fall are converted to halo masses by multiplying the former by 9.4 (20) for spirals (ellipticals), keeping L/M constant (see text). Left panel: equiprobability contours are drawn at $\log[\mathcal{L}_f \, \mathcal{P}(M, \mathcal{L}_f/M) \, \ln(10.)^2] = -5, \ldots, -2$. Dashed line indicates the scaling $\mathcal{L}_f \propto M^{5/3}$, which follows from the dimensional dependence $\mathcal{L}_* \propto M_*^{5/3}$. The theoretical equiprobability contours correspond to a single smoothing scale R_*, chosen such that $M_* = 1.74 \times 10^{11} \, M_\odot$ for $h = 0.5$. Right panel: same as left panel but for peaks with height $1/2 \leq \nu \leq 3/2$ (dotted contours) and $3/2 \leq \nu \leq 5/2$ (continuous contours).

Our prediction for the dimensional value for $\mathcal{L}_f/M$ versus M on the scale of a rich cluster of galaxies is depicted in Fig. 10. Selecting objects of masses comparable to such structures leads to typical $\mathcal{L}_f/M$ values one order of magnitude larger than for spiral galaxies. Note that the importance of both non-linear interactions and dissipation are less likely to affect this prediction than in the comparison with galaxies.

Our estimate of the specific angular momentum can also be compared against results from numerical simulations. However, the status of those simulations seems to be slightly controversial. For instance, Zurek, Quinn & Salmon (1988) find values of the specific angular momentum in agreement with spiral galaxies, but too high for ellipticals (e.g. their Fig. 2), yet in the calculations of Navarro, Frenk & White (1995, Fig. 10), values of L/M are found consistent with elliptical galaxies but too low for spirals. Note that these latter authors have included dissipation and find that a substantial part of the angular momentum of the dissipating gas is lost to the surrounding halo. However, even their halos have L/M too low to fall in the region of spiral galaxies, making the discrepancy between these sets of simulations even worse. Franx, Illingworth & de Zeeuw (1991) have voiced the concern that numerical simulations might lack the dynamic range to be able to describe accurately the problem at hand. Having a simulation box of size Δ and Nyquist wavelength $\sim 1/R$ amounts to changing the effective width of the input power spectrum and hence has the tendency to change γ. This effect is illustrated in Fig. 11, which shows γ for given box size Δ and smoothing scale R. The bigger box simulation with $R = 1$ Mpc reaches the asymptotic CDM input value $\gamma = 0.62$. Referring to Fig. 7, it is clear that simulations with *identical* physical spectrum but different dynamic range may lead to values of the typical angular momentum differing by factors of a few, especially for rare events.

4.3   Rotational velocities versus scale

We can obtain estimates for the rotational velocity from our values of the angular momentum as a function of mass, for scales corresponding to galaxies, clusters and superclusters. The angular momentum derived from equation (31) gives typical values $\mathcal{L}_f \approx 1.8 \times 10^{67}$ kg m^2 s^{-1} for a $\nu = 1$ peak, using the median value $\overline{\ell_f} = 5.3$ appropriate for a CDM $\gamma = 0.62$, for $h = 0.5$, $z_1 = 3$ and $M_* = 1.84 \times 10^{10} h^{-1} M_\odot$ (corresponding to a Milky Way mass $1.1 \times 10^{11} \, M_\odot$), well in line with previous estimates for the Galaxy: Peebles (1969) quotes for the Milky Way a value 2.4×10^{67} kg m^2 s^{-1}, comparable to the estimate of Fall & Efstathiou (1980). This translates to a circular velocity $v_R = \mathcal{L}_f/MR \approx 140$ km s^{-1}, using $M = 1.1 \times 10^{11} M_\odot$ and
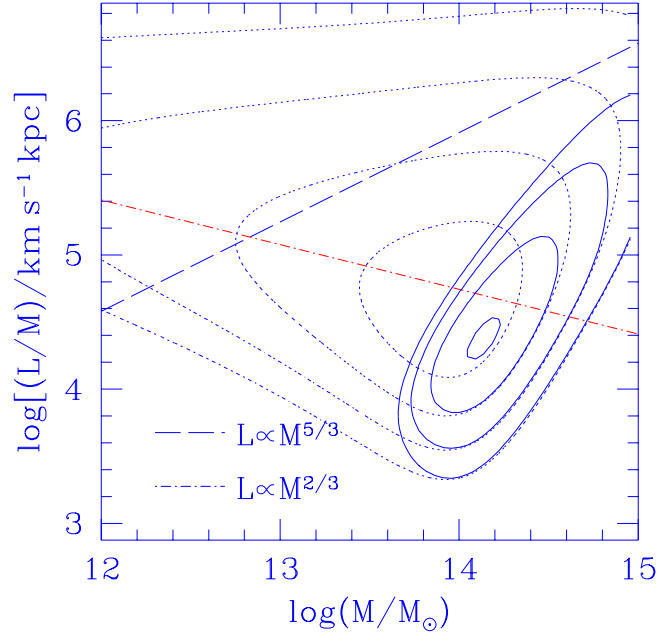
Figure 10. Equiprobability contours of specific angular momentum versus mass, using a smoothing scale such that $M_* = 1.16 \times 10^{13}\, M_\odot$ for $h = 0.5$ appropriate for rich Abell clusters. Dotted contours refer to all objects whereas continuous contours refer to the subset $5/2 \leq \nu \leq 9/2$. Contour levels are -5, -4, -3, -2.2. These specific angular momenta correspond to rotational velocities $\approx 5\,\mathrm{km\,s^{-1}}$, on cluster scales of 3 Mpc
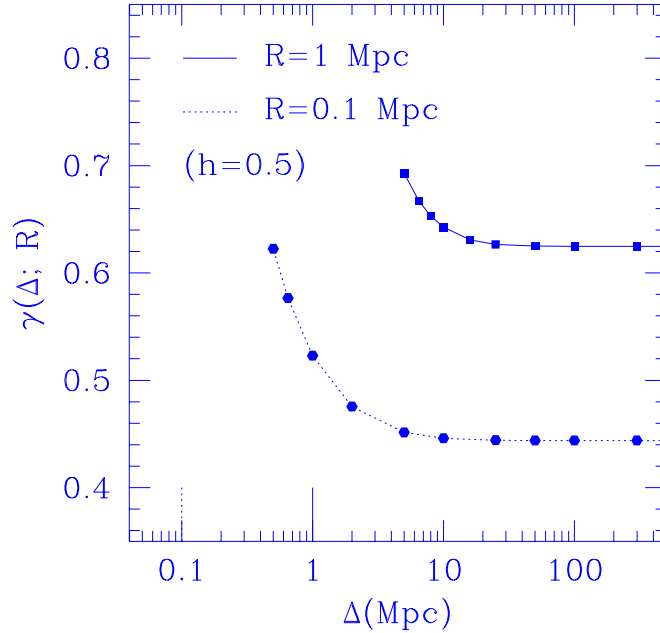

Figure 11. Effective value of the spectral parameter γ for a CDM simulation of box size Δ and resolution R. The input CDM spectrum is from the fit (7.10) in Efstathiou (1989).

$R = 20\,\text{kpc}$. Applying the same method, we proceed to compute the typical circular velocity of structures on larger scales. For a rich cluster of mass $\sim 10^{14} M_\odot$ and size $R \sim 3$ Mpc, we find $v_R \approx 1.5 \times 10^4 \text{ km s}^{-1} \text{ kpc}/3\,\text{Mpc} \approx 5\,\text{km s}^{-1}$, where we used the most likely value of $\mathcal{L}_f/M$ read from Fig. 10 for $\nu \sim 3$. This very low value is clearly consistent with the lack of observational evidence for cluster rotation (Efstathiou & Barnes 1984). For a supercluster of mass $10^{16} M_\odot$ we use the simple scaling $v_R \sim 5\,(\rho_{sc}/\rho_c)^{1/3}\,(M_{sc}/M_c)^{1/3} \approx 10\,\text{km s}^{-1}$, taking the density of the supercluster to be equal to the background density and the density and mass of a typical galaxy cluster as previously. Note that these structures are likely to be still in the linear regime, hence this value must be decreased by the fraction t/t_M of the age of the Universe in units of the turnaround time of the supercluster. Furthermore, the spherical approximation is clearly poor to describe the structures on supercluster scales, hence this estimate of $v_R(\text{sc})$ must be considered rather uncertain.

5 SUMMARY AND CONCLUSIONS

In this paper we re-analyzed the problem of the acquisition of angular momentum by a protoobject, progenitor of a galaxy or a cluster, due to tidal interactions with the surrounding matter distribution. This process is of most interest for gravitational instability theories of galaxy and cluster formation. In section 2, we reviewed the dynamical description of the spin evolution in the version given by White (1984), hence the motion of the matter patch of fluid is followed by applying the Zel'dovich approximation. The expression for the linear tidal angular momentum $\mathbf{L}$ of a protoobject obtained in this formalism and reported in equation (7), contains a combination of the deformation tensor $\mathcal{D}_{\alpha\beta}$ and the inertia tensor $\mathcal{J}_{\alpha\beta}$ of the matter inside the Lagrangian volume Γ, which by definition encloses the collapsing protoobject. Such a combination of the elements of the tensors $\mathcal{D}$ and $\mathcal{J}$ is zero if Γ is a spherical volume (or if the boundary of Γ is an equipotential of the gravitational potential). The temporal evolution of the spin is governed in the linear regime by the function $a(t)^2\,\dot{D}(t)$, where $a(t)$ is the scale factor and $D(t)$ is the growth factor of the linear density perturbations, which is proportional to the cosmic time t in the Einstein-de Sitter universe (Doroshkevich 1970).

These results may be notably simplified by considering the ensemble expectation value of the square of the angular momentum $\langle \mathbf{L}^2 \rangle$. The resulting general (albeit approximate) expression in equation (16) is one of the main results of this paper. It highlights the very simple fact that, in linear regime, the ensemble average $\langle \mathbf{L}^2 \rangle$ is a function of the first and second invariant of the inertia tensor $\mathcal{J}$ alone and is in addition proportional to the mass variance $\sigma_0(R)^2$ on the scale R. The fact that $\langle \mathbf{L}^2 \rangle$ depends only on the invariants of the inertia tensor and not on the detailed shape of the surface boundary of Γ provides a considerable simplification of the calculation.

In section 2.3, we specialised the statistic $\langle \mathbf{L}^2 \rangle$ to the case in which the volume Γ is centered on a peak of the underlying Gaussian density field. The ensemble average is therefore restricted to those realizations of the density field that are compatible with the preselected shape of the collapsing object. This constrained ensemble average corresponds to an unconstrained ensemble average over the off-diagonal shear (see the extensive discussion in Appendix B). The analysis of the tidal torques acting on matter in the vicinity of local density maxima (peaks) during the linear regime has been first attempted by Hoffman (1986; 1988) and Heavens & Peacock (1988). In particular, Hoffman first analyzed the correlation between the height ν of the peak and the amount of angular momentum it acquires by tidal interactions. Heavens & Peacock performed a more sophisticated investigation, taking into account also the asymmetric shape of the matter peak, described in terms of the eigenvalues $-\lambda_1, -\lambda_2, -\lambda_3$ of the mass tensor $\partial_\alpha \partial_\beta \delta$ (Bardeen et al. 1986). This represents an important improvement because the strength of the tidal interactions depends strongly on the shape of the object. Our analysis uses an approach complementary to the one of Heavens and Peacock and extends their work.

The resulting expression for $\langle \mathbf{L}^2 \rangle$ appropriate for peaks has been recast in equation (19) into two factors: $\mathcal{L} \equiv \sqrt{\langle \mathbf{L}^2 \rangle} = \ell \mathcal{L}_*$, where $\ell = \ell(\nu, x, e, p; \gamma)$ is dimensionless and contains the dependence on peak shape (height ν, sharpness x, ellipticity e and prolateness p) and $\mathcal{L}_* = \mathcal{L}_*(t; R_*)$ is the angular momentum unit which contains the growth rate and is fixed by the cut-off R_* of the power spectrum. This factorization should be compared with the one in Heavens & Peacock (1988) for the modulus J of the angular momentum, their equation (9), which corresponds to a single realisation of the shear field. We then proceed by computing the probability distribution of several spin variables (e.g. of ℓ, ℓ/m, $\ell/m^{5/3}$ versus mass m of the peak; m is the dimensionless mass of the peak in units of the mass selected by R_*) by using the probability distribution of peak shape parameters (Bardeen et al. 1986). This is an important extension of the work of Heavens & Peacock (1988), who analysed the rotational properties of galaxies directly in terms of spin parameters versus the peak height ν. The latter, however, does not allow to determine uniquely the mass-scale of the progenitor. As we argued at the end of section 2.3, we expect our distributions of angular momentum versus mass to be more reliable than the estimates for single objects.

In sections 3 and 4, we computed and discussed probability distributions for ℓ, ℓ/m and $\ell/m^{5/3}$ and the dimensionless spin parameter λ, both in linear regime and at the time of maximum expansion. Our findings can be summarized as follows:

- linear values of the spin ℓ have a strong dependence on m: $\ell \propto m^{5/3}$, see Fig. 1
- for objects of a restricted range in ν, this dependence steepens to $\ell \propto m^{8/3}$, see Fig. 2
- final values (i.e., at maximum expansion time) ℓ_f of ℓ scale shallower with m, $\ell_f \propto m^{2/3}$, see Fig. 6

• median values of ℓ_f decrease with ν for high γ (i.e. steep spectra) but are rather insensitive to ν for low γ (i.e. broad spectra)

• median values of ℓ_f decrease with γ for given ν

• median values for λ are $\overline{\lambda}(\nu = 1) = 0.15$ and $\overline{\lambda}(\nu = 2) = 0.07$, comfortably close to the spin of spiral galaxies but marginally higher than the value typically quoted for ellipticals

• dimensional values of $\mathcal{L}_f/M$ on galactic scales are in good agreement with measured values for spirals but are too high to described ellipticals

• selecting objects on galactic scales with peak height $\nu \sim 1$ gives values of $\mathcal{L}_f/M$ typical of spiral galaxies. Selecting objects with $\nu \sim 2$ moves the position of the most probable $\mathcal{L}_f/M$ in the direction of the location of elliptical galaxies in the $(M, \mathcal{L}_f/M)$ plane but the shift falls short by a large margin to give good agreement between values of $\mathcal{L}_f/M$ for $\nu = 2$ peaks and those observed for ellipticals.

• typical values of the angular momentum of a spiral galaxy are predicted to be $\mathcal{L}_f \approx 1.8 \times 10^{67}\,\text{kg m}^2\,\text{s}^{-1}$ with a corresponding circular velocity $v_{c,\text{spiral}} \approx 140\,\text{km s}^{-1}$. For a rich cluster, we find a typical value $v_{c,\text{clus.}} \approx 5\,\text{km s}^{-1}$ while for a supercluster $v_{c,\text{sup.clus.}} \leq 10\,\text{km s}^{-1}$.

The reliability of our estimate for the ensemble averaged value $\Lambda_f \equiv \sqrt{\langle \lambda_f^2 \rangle}$ depends on the extent to which our approximations capture the main features of the dominant processes. We have made the following assumptions: (1) linear perturbation theory, extrapolated to the mildly non-linear regime (Zel'dovich approximation), can be used to describe the growth of ℓ until the maximum expansion time ; (2) tidal torques spin up the matter until the maximum expansion time of the protoobject and are negligible thereafter; (3) the mass of the object can be identified with the mass inside an isodensity ellipsoidal surface around the peak; (4) the spherical model can be used to calculate the clump's binding energy E – needed to compute λ; (5) Gaussian peaks formalism (Bardeen et al. 1986) can be used to compute probability distributions for ℓ_β.

We briefly comment on the appropriateness of these approximations. The use of the Zel'dovich approximation, very powerful in describing the mildly non-linear evolution of matter before shell-crossing, may give only a partial description of the evolution of the tidal angular momentum of the clumps themselves. Certainly, it cannot predict the very final stages of evolution when clumps merge and interact non-linearly, which leads to the present-day galactic configurations. In fact, as shown by the numerical simulations of e.g. Barnes & Efstathiou (1987), Frenk (1987), Zurek, Quinn & Salmon (1988), Navarro & Benz (1991) and Navarro & White (1994), the tidally acquired spin may change drastically as objects merge or as angular momentum gets transported between core and halo. The merging history of the surrounding protohalo is a key factor in the determination of the morphology of a galaxy and the merging processes of dense clumps are associated with substantial *loss* of angular momentum to the halo. $\mathcal{L}_f$ – as obtained from the extrapolation of the linear theory – is typically a factor of ~ 3 larger than the final spin of the non-linear object (Barnes & Efstathiou 1987; Frenk 1987). At present, we see little hope of computing theoretically such a reduction factor, which is due to non-linear interactions as well as late infall and dissipation processes. Consequently, these processes constrain the applicability of perturbation theory to the period before the maximum expansion time (Catelan & Theuns 1996).

The determination of the surface boundary of the Lagrangian volume Γ is tricky. This boundary determines the mass of the object. We assumed that it can be described by an isodensity contour, which is ellipsoidal when the object is centered on a high peak. However, a non-negligible part of the luminous matter might have been captured from the very outer regions of the proto-galaxies (Ryden 1988; Quinn & Binney 1992), where the ellipsoidal model is presumably a poor description. In addition, the formalism applied here is also based on Taylor expanding the density and the velocity fields around the centre of the peak. This expansion breaks down far from the peak's centre and consequently is unable to accommodate late infall (see the discussion in Hoffman 1988), a process definitely important during the late stages of galaxy formation (e.g. Navarro & White 1994).

In assuming the spherical model to estimate the clump's binding energy E, we have lost the explicit dependence of E on the properties of the underlying linear gravitational potential field ψ. Consequently, our calculation could be improved by taking this dependence into account (see Hoffman 1988, section II), but this would complicate considerably the computation of the ensemble average and is beyond the scope of the present paper.

Finally, in comparing our predictions against measurements of luminous parts of galaxies, one has to bear in mind that dissipative processes, not taken into account here, surely have had a major influence in shaping those objects.

REFERENCES

Bardeen J.M., Bond J.R., Kaiser N., Szalay A.S., 1986, ApJ, 304,15
Barnes J. & Efstathiou G., 1987, ApJ, 319, 575
Bertschinger E., 1987, ApJ, 323, L103
Binney J.J., 1978, MNRAS, 183, 501
Blumenthal G.R., Faber S.M., Primack J.R. & Rees M., 1984, Nature, 311, 517
Bouchet F.R., Juszkiewicz R., Colombi S. & Pellat R., 1992, ApJ, 394, L5
Buchert T., 1994, MNRAS, 267, 811
Catelan P., 1995, MNRAS, 276, 115
Catelan P. & Theuns T., 1996, MNRAS, to be published
Couchman H.M.P., 1987, MNRAS, 225, 795
Davies R., Efstathiou G., Fall S.M., Illingworth G. & Schechter P., 1983, ApJ, 266, 41
Doroshkevich A.G., 1970, Astrofizika, 6, 581
Efstathiou G. & Barnes J., 1984, in *Formation and Evolution of Galaxies and Large Structures in the Universe*, eds. Audouze J. and
    Tran Thanh Van J., (Reidel, Dordrecht)
Efstathiou G., 1989, in *Physics of the Early Universe*, edts. Peacock J.A., Heavens A.F. & Davies A.T. (Edinburgh University Press)
Efstathiou G. & Jones B.J.T., 1979, MNRAS, 186, 133
Eisenstein D.J. & Loeb A., 1995, ApJ, 439, 520
Faber S., 1982, in *Astrophysical Cosmology*, eds. Brück H.A., Coyne G.V. & Longair M.S. (Princeton University Press)
Fall S.M., 1983, in *Internal Kinematics and Dynamics of Galaxies*, IAU Symposium 100, ed. Athanassoula E. (Dordrecht, Reidel)
Fall S.M. & Efstathiou G., 1980, MNRAS, 193, 189
Franx, M., Illingworth, G. & de Zeeuw, T., 1991, ApJ, 327, 383
Frenk, C.S., 1987, in *Nearly Normal Galaxies: from the Planck time to the present*, ed. Faber, S., (New York, Springer-Verlag)
Heavens A. & Peacock J., 1988, MNRAS, 232, 339
Hoffman Y., 1986, ApJ, 301, 65
Hoffman Y., 1988, ApJ, 329, 8
Hoffman Y. & Ribak E., 1991, ApJ, 380, L5
Hoyle F., 1949, in *Problems of Cosmical Aerodynamics*, eds. Burgers J.M. & van de Hulst H.C. (Central Air Documents Office, Dayton).
Kormendy J. & Illingworth G., 1982, ApJ, 256, 460
Illingworth G. & Schechter P.L., 1982, ApJ, 256, 481
Kaiser N., 1984, ApJ, 284, L9
Kashlinsky A., 1982, MNRAS, 200, 585
Kofman L., 1991, in *Primordial Nucleosynthesis and Evolution of the Early Universe*, ed. Sato, K., Dordrecht: Kluwer Academic
Navarro J.F. & Benz W., 1991, ApJ, 380, 320
Navarro J.F. & White S.D.M., 1994, MNRAS, 267, 401
Navarro J.F., Frenk C.S. & White S.D.M., 1995, MNRAS, 275, 56
Peacock J.A., Heavens A.F., 1985, MNRAS, 217, 805
Peacock J.A., Heavens A.F., 1990, MNRAS, 243, 133
Peebles P.J.E., 1969, ApJ, 155, 393
Peebles P.J.E., 1971, A&A, 11, 377
Peebles P.J.E., 1980, The Large–Scale Structure of the Universe, Princeton University Press, Princeton
Politzer H.D., Wise M.B., 1984, ApJ, 285, L1
Quinn T. & Binney J., 1992, MNRAS, 255, 729
Ryden B.S., 1988, ApJ, 329, 589
Sandage A., Freeman K. & Stokes N.R., 1970, ApJ, 160, 831
Sciama D.W., 1955, MNRAS, 115, 3
Shandarin S.F. & Zel'dovich Ya.B. 1989, Rev. Mod. Phys., 61, 185
Sheth R.K., 1995, MNRAS, 277, 933
Steinmetz M. & Bartelmann M., 1995, MNRAS, 272, 570
van de Weygaert R. & Bertschinger E., 1996, MNRAS, to be published
Warren M.S., Quinn P.J., Salmon J.K. & Zurek W.H., 1992, ApJ, 399, 405
White S.D.M., 1984, ApJ, 286, 38
White S.D.M., 1994, MPA preprint 831
Zel'dovich Ya.B., 1970a, A&A, 5, 84
Zel'dovich Ya.B., 1970b, Astrophysics, 6, 164
Zurek W.H., Quinn, P.J. & Salmon, J.K., ApJ, 330, 519

APPENDIX A

In this first appendix, we show explicitly how to derive equation (16). The expression in equation (14) may be concisely written as

$$\langle \mathcal{D}_{\beta\sigma} \mathcal{D}_{\beta'\sigma'} \rangle_\psi = (\delta_{\beta\sigma}\,\delta_{\beta'\sigma'} + \delta_{\beta\beta'}\,\delta_{\sigma\sigma'} + \delta_{\beta\sigma'}\,\delta_{\beta'\sigma})\,\Phi \,, \tag{38}$$

where we have defined

$$\Phi \equiv \frac{4\pi}{15(2\pi)^3} \int_0^\infty dp\, p^6\, P_\psi(p)\, \widetilde{W}(pR)^2 = \frac{\sigma_0^2}{15}\,. \tag{39}$$

Then, from (13)

$$
\begin{aligned}
\langle \mathbf{L}^2 \rangle &= a^4 \dot{D}^2\,\Phi\,\epsilon_{\alpha\beta\gamma}\,\epsilon_{\alpha\beta'\gamma'}\,\mathcal{J}_{\sigma\gamma}\,\mathcal{J}_{\sigma'\gamma'}\,(\delta_{\beta\sigma}\,\delta_{\beta'\sigma'} + \delta_{\beta\beta'}\,\delta_{\sigma\sigma'} + \delta_{\beta\sigma'}\,\delta_{\beta'\sigma}) \\
&= a^4 \dot{D}^2\,\Phi\,(\epsilon_{\alpha\beta\gamma}\,\epsilon_{\alpha\beta\gamma'}\,\mathcal{J}_{\sigma\gamma'} + \epsilon_{\alpha\sigma\gamma}\,\epsilon_{\alpha\sigma'\gamma'}\,\mathcal{J}_{\sigma'\gamma'} + \epsilon_{\alpha\beta\gamma}\,\epsilon_{\alpha\sigma\gamma'}\,\mathcal{J}_{\beta\gamma'})\,\mathcal{J}_{\sigma\gamma} \\
&= a^4 \dot{D}^2\,\Phi\,[2\,\delta_{\gamma\gamma'}\,\mathcal{J}_{\sigma\gamma'} + (\delta_{\beta\sigma}\,\delta_{\gamma\gamma'} - \delta_{\beta\gamma'}\,\delta_{\gamma\sigma})\,\mathcal{J}_{\beta\gamma'}]\,\mathcal{J}_{\sigma\gamma} \\
&= a^4 \dot{D}^2\,\Phi\,[3\,\mathcal{J}_{\alpha\beta}\,\mathcal{J}_{\alpha\beta} - (\mathcal{J}_{\alpha\alpha})^2]\,.
\end{aligned}
\tag{40}
$$

This scalar expression does not depend on the particular coordinate system: let us suppose that the axes coincide with the principal axes of the inertia tensor; then

$$(\mathcal{J}_{\alpha\beta}) \equiv \mathrm{diag}(\iota_1, \iota_2, \iota_3)\,, \tag{41}$$

thus $3\,\mathcal{J}_{\alpha\beta}\,\mathcal{J}_{\alpha\beta} - (\mathcal{J}_{\alpha\alpha})^2 = 2\,(\mu_1^2 - 3\mu_2)$, where μ_1 and μ_2 are respectively the first and the second invariants of the inertia tensor, namely $\mu_1 \equiv \mathrm{Tr}(\mathcal{J}) = \iota_1 + \iota_2 + \iota_3$ and $\mu_2 \equiv \iota_1\iota_2 + \iota_1\iota_3 + \iota_2\iota_3$. Finally, the equation (16) is obtained. We stress that this result holds for any given Lagrangian volume Γ whose inertia tensor is characterised by the eigenvalues ι_α.

APPENDIX B

In this second appendix, we show more in detail how to specialize the ensemble average $\langle \mathbf{L}^2 \rangle_\psi$ to the case in which the volume Γ is centered on a peak of the density field: it turns out that combination of eigenvalues $\mu_1^2 - 3\mu_2$ depends on the parameters characterizing the shape of the peak.

We assume that the isodensity profile $\delta_c = 0$ is the boundary surface of the Lagrangian volume Γ: such a boundary is approximately simply connected and ellipsoidal, at least for sufficiently high density peaks (Doroshkevich 1970; Bardeen et al. 1986; Couchman 1987).

A density peak is characterised by the conditions $\nabla\delta = \mathbf{0}$ and the tensor $\partial_\alpha\partial_\beta\delta$ has to be negative definite: the location of the peak is assumed to coincide with the origin $\mathbf{q} = \mathbf{0}$. In the vicinity of the maximum, and in the coordinate system oriented along the principal axes of the tensor $\partial_\alpha\partial_\beta\delta$, the density field is approximately described by the first three terms of the Taylor expansion (Bardeen et al. 1986):

$$\delta(\mathbf{q}) = \delta(\mathbf{0}) - \frac{1}{2}\sum_\alpha \lambda_\alpha q_\alpha^2\,, \tag{42}$$

where λ_α, $\alpha = 1, 2, 3$ are the eigenvalues of the tensor $-\partial_\alpha\partial_\beta\delta$: in such a case, each λ_α is positive in correspondence of a maximum, and it can be assumed that, e.g., $\lambda_1 \geq \lambda_2 \geq \lambda_3 > 0$. Expressing the height of the peak in units of σ_0, $\delta(\mathbf{0}) \equiv \nu\sigma_0$, the surface boundary of Γ may be written as

$$\frac{q_1^2}{A_1^2} + \frac{q_2^2}{A_2^2} + \frac{q_3^2}{A_3^2} = 1\,, \tag{43}$$

where the quantities A_α are the principal semi–axes of the ellipsoidal isodensity surface $\delta_c = 0$:

$$A_\alpha^2 = \frac{2\nu\sigma_0}{\lambda_\alpha}\,. \tag{44}$$

At this point, noting that if the tensor $\partial_\alpha\partial_\beta\delta$ is diagonal, the inertia tensor $\mathcal{J}_{\alpha\beta}$ is diagonal as well,

$$(\mathcal{J}_{\alpha\beta}) = \mathrm{diag}(\iota_1, \iota_2, \iota_3) = \frac{1}{5}\,\eta_0\,\Gamma\,\mathrm{diag}(A_1^2, A_2^2, A_3^2)\,, \tag{45}$$

it is straightforward to show that the combination $\mu_1^2 - 3\mu_2$ reduces to

$$\mu_1^2 - 3\mu_2 = 2^{11}\,3^4\,5^{-2}\,\pi^2\,\eta_0^2\,\left(\frac{\nu}{x}\right)^5\left(\frac{\sigma_0}{\sigma_2}\right)^5\,\frac{\mathcal{A}(e,p)}{\mathcal{B}(e,p)^3}\,, \tag{46}$$

where we have introduced the polynomials

$$\mathcal{A}(e,p) \equiv [p(1+p)]^2 + 3e^2(1 - 6p + 2p^2 + 3e^2)\,, \tag{47}$$

and

$$\mathcal{B}(e,p) \equiv (1 - 2p)\,[(1+p)^2 - 9e^2]\,, \tag{48}$$

and the relation $\Gamma = \frac{4\pi}{3} A_1 A_2 A_3$ has to be used.

The parameter $x \equiv -\sigma_2^{-1} \nabla^2 \delta = \sigma_2^{-1}(\lambda_1 + \lambda_2 + \lambda_3)$ is an indicator of the 'sharpness' of the peak; the quantity σ_2 is related to the variance of the field $\partial_\alpha \partial_\beta \delta$ and it is an element of a set of spectral parameters weighted by powers of the wavevector squared, k^2,

$$\sigma_h(R)^2 \equiv \int_0^\infty \frac{dk\, k^6}{2\pi^2}\, k^{2h}\, P_\psi(k) \widetilde{W}(kR)^2 \ . \tag{49}$$

It results that $\langle k^2 \rangle = \sigma_1^2/\sigma_0^2$ and $\langle k^4 \rangle = \sigma_2^2/\sigma_0^2$. The parameters e and p characterize the asymmetry of the isodensity profile:

$$e \equiv \frac{\lambda_1 - \lambda_3}{2(\lambda_1 + \lambda_2 + \lambda_3)} = \frac{\lambda_1 - \lambda_3}{2\, x\, \sigma_2} \ , \tag{50}$$

$$p \equiv \frac{\lambda_1 - 2\lambda_2 + \lambda_3}{2(\lambda_1 + \lambda_2 + \lambda_3)} = \frac{\lambda_1 - 2\lambda_2 + \lambda_3}{2\, x\, \sigma_2} \ ; \tag{51}$$

also

$$\lambda_1 = \frac{1}{3}\sigma_2\, x\, (1 + p + 3e) \ , \tag{52}$$

$$\lambda_2 = \frac{1}{3}\sigma_2\, x\, (1 - 2p) \ , \tag{53}$$

$$\lambda_3 = \frac{1}{3}\sigma_2\, x\, (1 + p - 3e) \ . \tag{54}$$

More in detail, the parameter $e (\geq 0)$ measures the *ellipticity* of the matter distribution in the plane (q_1, q_3), while p determines the *oblateness* $(0 \leq p \leq e)$ or the *prolateness* $(-e \leq p \leq 0)$ of the triaxial ellipsoid. If $e > 0$, then spheroids with $p = e$ are said to be oblate, while spheroids with $p = -e$ are said to be prolate; if $e = 0$, then $p = 0$, the ellipsoid is a sphere: however, spherical peaks are strongly improbable (see Bardeen et al. 1986 for more details).

Finally, the ratio σ_0/σ_2 in equation (46) may be written in terms of two further relevant spectral parameters, γ and R_*:

$$\gamma \equiv \langle x\nu \rangle = \frac{\sigma_1^2}{\sigma_0\, \sigma_2} \ , \tag{55}$$

$$R_* \equiv \sqrt{3}\, \frac{\sigma_1}{\sigma_2} \ . \tag{56}$$

The meaning of these statistics is the following: the parameter γ is a measure of the width of the power spectrum, since

$$\sqrt{\frac{\langle (k^2 - \langle k^2 \rangle)^2 \rangle}{\langle k^2 \rangle^2}} = \sqrt{\frac{1}{\gamma^2} - 1} \tag{57}$$

measures the relative spectral width: if the spectrum is a delta function, then $\gamma = 1$; on the contrary, if $k^7 P_\psi(k)$ is constant over a wide range of k, then $\gamma \ll 1$; the dependence of γ on the scale for a Cold Dark Matter power spectrum is displayed in Fig. 1 of Bardeen et al. (1986): typically, on galactic scale, $\gamma = 0.62$. The parameter R_* is a measure of the coherence scale in the field or, in other words, it gives an indication of the smallest wavelength in the power spectrum (see the corresponding discussion in the main text).

Inserting the relation $\sigma_0/\sigma_2 = R_*^2/3\gamma$ in equation (46), and using the general expression (16) for the ensemble average $\langle \mathbf{L}^2 \rangle_\psi$, and the expression for the volume Γ, we obtain

$$\langle \mathbf{L}^2 \rangle_\psi = \frac{2^{12}\, 3\, \pi^2}{15^3}\, a^4\, \dot{D}^2\, \eta_0^2\, \sigma_0^2\, R_*^{10} \left(\frac{\nu}{\gamma x} \right)^5 \frac{\mathcal{A}(e, p)}{\mathcal{B}(e, p)^3} \ . \tag{58}$$

This is an interesting expression: since we *first* calculated the ensemble average, we have been able to write the expectation value $\langle \mathbf{L}^2 \rangle_\psi$ as a function of the four peak pattern parameters ν, x, e, p. Following the suggestion in Heavens & Peacock (1988), we can write the previous expression as

$$\mathcal{L} \equiv \sqrt{\langle \mathbf{L}^2 \rangle} = \ell\, \mathcal{L}_* \ , \tag{59}$$

where we have defined

$$\mathcal{L}_* \equiv a^2 \dot{D}\, \eta_0\, \sigma_0\, R_*^5 \ , \tag{60}$$

and

$$\ell \equiv \frac{96\, \pi}{\sqrt{15^3}} \left(\frac{\nu}{\gamma x} \right)^{5/2} \frac{\mathcal{A}(e, p)^{1/2}}{\mathcal{B}(e, p)^{3/2}} \ . \tag{61}$$

The significance of the quantities ℓ and $\mathcal{L}_*$ is discussed in the main text.

The probability distribution $\mathcal{P}(\nu, x, e, p)\, d\nu\, dx\, de\, dp$ of the peak shape parameters has been obtained by Bardeen et al. (1986): it reads

$$\mathcal{P}(\nu, x, e, p) = \mathcal{P}_0 \, x^8 \, \mathcal{W}(e,p) \, \exp\left[-\frac{\nu^2}{2} - \frac{5}{2}x^2(3e^2 + p^2) - \frac{(x - \gamma\nu)^2}{2(1-\gamma^2)} \right] \,, \tag{62}$$

in the allowed domain (a triangle) $0 \le e \le \frac{1}{4}$, $-e \le p \le e$ and $\frac{1}{4} \le e \le \frac{1}{2}$, $3e-1 \le p \le e$, and by definition vanishing outside of the triangle. The normalization constant is $\mathcal{P}_0 \equiv 3^2 5^{5/2}/(2\pi)^3 R_*^3 \, (1-\gamma^2)^{1/2}$ and the function $\mathcal{W}(e,p) \equiv e(e^2 - p^2)\,\mathcal{B}(e,p)$.

We stress the fact that the multiplicative factor $(1-\gamma^2)^{1/2}$ appearing in equation (21), but still missing in equation (61), can not be obtained by the procedure outlined so far. The origin of this factor is as follows. The procedure outlined so far is equivalent to preselecting a volume Γ with a given inertia tensor and *independently* assigning the realisation of ψ, hence neglecting the fact that the inertia tensor is in general statistically correlated with ψ. To obtain consistent results when studying objects with a *given* inertia tensor, the ensemble average of $\mathbf{L}^2$ should *not* be calculated over the realizations of the *unconstrained* potential ψ (as we have done so far – see section 2.2), but only over those realizations of ψ which are compatible with the preselected Γ. In general, this is a hugely difficult calculation to perform. Fortunately, in the framework of the Gaussian peak model, this can be done both consistently and easily, in that the angular momentum is determined by the *off-diagonal* components of the shear field $\mathcal{D}_{\alpha\beta}$ only, and the latter turn out to be statistically *independent* of the shape of the peak (i.e., of its inertia tensor). Consequently, as far as the angular momentum is concerned, to compute the ensemble average over the constrained potential field, $\langle \cdot \rangle_{\psi|\mathcal{J}}$, it is enough to compute the ensemble average over the off-diagonal (unconstrained!) shear components, $\langle \cdot \rangle_{\mathcal{D}_{od}}$.

More in detail, the joint distribution of the shape parameters of Gaussian peaks and the off-diagonal shear components is given by (see equation (A24) in Heavens & Peacock 1988):

$$\mathcal{P}(\nu, x, e, p, \mathcal{D}_{12}, \mathcal{D}_{13}, \mathcal{D}_{23}) = \mathcal{P}(\nu, x, e, p) \, \mathcal{P}(\mathcal{D}_{12}, \mathcal{D}_{13}, \mathcal{D}_{23}) \,, \tag{63}$$

where the $\mathcal{D}$ are Gaussian distributed with zero mean and variance $\sigma_{\mathcal{D}}^2 = \sigma_0^2 \, (1 - \gamma^2)/15$:

$$\mathcal{P}(\mathcal{D}_{12}, \mathcal{D}_{13}, \mathcal{D}_{23}) = \left(2\pi \, \sigma_{\mathcal{D}}^2\right)^{-3/2} \exp[-(\mathcal{D}_{12}^2 + \mathcal{D}_{13}^2 + \mathcal{D}_{23}^2)/2\,\sigma_{\mathcal{D}}^2] \,. \tag{64}$$

Note that in equation (38) we have computed the ensemble average over the (unconstrained) potential field ψ, leading to a dispersion

$$\langle \mathcal{D}_{\beta\sigma} \mathcal{D}_{\beta'\sigma'} \rangle_\psi = (\delta_{\beta\sigma} \, \delta_{\beta'\sigma'} + \delta_{\beta\beta'} \, \delta_{\sigma\sigma'} + \delta_{\beta\sigma'} \, \delta_{\beta'\sigma}) \, \frac{\sigma_0^2}{15} \,, \tag{65}$$

whereas computing the ensemble average over the off-diagonal shear (which is equivalent to computing the average over the constrained potential field) we now find:

$$\langle \mathcal{D}_{\beta\sigma} \mathcal{D}_{\beta'\sigma'} \rangle_{\psi|\mathcal{J}} = \langle \mathcal{D}_{\beta\sigma} \mathcal{D}_{\beta'\sigma'} \rangle_{\mathcal{D}_{od}} = (\delta_{\beta\sigma} \, \delta_{\beta'\sigma'} + \delta_{\beta\beta'} \, \delta_{\sigma\sigma'} + \delta_{\beta\sigma'} \, \delta_{\beta'\sigma}) \, \frac{(1-\gamma^2)\,\sigma_0^2}{15} \,. \tag{66}$$

Repeating the calculation in Appendix A, but using $\Phi = \sigma_{\mathcal{D}}^2$, one recovers equation (21) instead of equation (61).

Intuitively, the smaller dispersion in the latter case makes sense: the random field is constrained to have a peak with specified shape, hence the dispersion of the shear tensor will be smaller than in the first, unconstrained case. This is the origin of the extra factor $(1-\gamma^2)^{1/2}$ appearing in equation (21): it properly takes into account the reduction in rms angular momentum because the reduction of the dispersion in shear due to the imposed constrained of having a peak with given shape.

A final remark: although the procedure outlined in section 2.2 is only approximate, it does have some important advantages when one tries to address fundamental issues related to the tidal torquing of the progenitors of the present structures. For instance, (*i*) how does the galactic tidal spin evolve during the non–linear regime? It is know, in fact, that even if the primordial fluctuations are Gaussian, the non–linear evolution will ensure that the mass–density fluctuations become highly non–Gaussian. The simple Gaussian peak model, for example, cannot be applied during the non–linear regime, yet the present approximate method can be applied (Catelan & Theuns 1996); (*ii*) how does the galactic tidal spin evolve during the non–linear regime starting from intrinsically non–Gaussian initial conditions? Again, the simple Gaussian peak model cannot be used (work in progress). The procedure suggested in section 2.2 could give some insight into these very complicated issues.

APPENDIX C

In this Appendix we give some technical details on how to compute some probability distribution functions, e.g. the one in equation (25). We start from the probability distribution $\mathcal{P}(\nu, x, e, p)$, given in equation (62). The distribution $P(m, \ell_\beta; \nu_1 \le \nu \le \nu_2)$ can be obtained from that by transforming $(e, p) \to (m, \ell_\beta)$. Technically, this can be done more easily in two steps, $(e, p) \to (\mathcal{A}, \mathcal{B})$ and $(\mathcal{A}, \mathcal{B}) \to (m, \ell_\beta)$, by using the quantities $\mathcal{A}$ and $\mathcal{B}$ as intermediate variables. To do this we first invert

the relations $\ell_\beta = \ell_\beta(\mathcal{A}, \mathcal{B})$ and $m = m(\mathcal{A}, \mathcal{B})$, using equations (21) and (22), to find:

$$\mathcal{A} = \left(\frac{\ell_\beta}{\ell_{\beta,0}}\right)^2 \left(\frac{m}{m_0}\right)^{2(\beta-3)} \left(\frac{\nu}{\gamma x}\right)^4 \tag{67}$$

$$\mathcal{B} = \left(\frac{m}{m_0}\right)^{-2} \left(\frac{\nu}{\gamma x}\right)^3 , \tag{68}$$

where $\ell_{\beta,0}$ and m_0 are numerical constants. One proceeds by computing the determinant of the Jacobian of the transformation, $(\mathcal{A}, \mathcal{B}) \rightarrow (m, \ell_\beta)$, which is $J_{\mathcal{AB}} = m\ell_\beta/4\mathcal{AB}$. On the other hand, $J_{ep} = 216e(e^2 - p^2)(1 - p^2 - 3e^3)$ is the determinant of the Jacobian of the transformation $(e, p) \rightarrow (\mathcal{A}, \mathcal{B})$. The parameters e and p occurring in J_{ep} have to be written in terms of $\mathcal{A}$ and $\mathcal{B}$, but this inversion $(e, p) \rightarrow (\mathcal{A}, \mathcal{B})$ cannot be performed analytically, as it involves finding the real roots of a polynomial of degree six! Combining these results, we find for the probability distribution:

$$\mathcal{P}(m, \ell_\beta; \nu_1 \leq \nu \leq \nu_2)\, dm\, d\ell_\beta = \left(\int_{\nu_1}^{\nu_2} d\nu \int_0^\infty dx\, \mathcal{P}[\nu, x, e(\nu, x, m, \ell_\beta), p(\nu, x, m, \ell_\beta)]\, J_{ep}^{-1}\, J_{\mathcal{AB}}^{-1}\right) dm\, d\ell_\beta . \tag{69}$$

One now observes that the inversion $(\mathcal{A}, \mathcal{B}) \rightarrow (m, \ell_\beta)$ only depends on the ratio $y \equiv \nu/x$ of the two variables ν and x. Hence, the foregoing expression can be simplified further in terms of y to give equation (25) quoted previously. The function $f(y)$ appearing in the argument of the exponential in that equation follows from equation (62), $f(y) = y^2/2 + 5(3e^2 + p^2)/2 + (1 - \gamma y)^2/2(1 - \gamma^2)$. One can now perform the integral over the peak sharpness x analytically, leaving a one dimensional numerical integration to obtain $\mathcal{P}(m, \ell_\beta; \nu_1 \leq \nu \leq \nu_2)$.

In some cases (e.g. to compute λ or ℓ_f) there is an extra ν dependence which makes that $\mathcal{A}$ and $\mathcal{B}$ do not depend on the ratio ν/x alone. In the computation of the distribution $\mathcal{P}(m, \ell_f/m^\beta)$, we eliminated ν and x in favour of m and ℓ_f/m^β, and $\mathcal{P}$ follows from a two dimensional integration over e and p. The computation of the λ distribution for given ν, on the other hand, can again be obtained from a one dimensional numerical integration, by transforming $(e, p) \rightarrow (m, \lambda)$ and noting that the latter change of variables only depends on $y \equiv m\, x^{3/2}$ and x, which allows one to compute the x integral analytically. We do not give the latter analytical expressions since they are rather cumbersome.